Title:

Solving the Coral Species Delimitation Conundrum

Authors:

Catalina Ramírez-Portilla[1, 2], Andrew H. Baird[3], Peter F. Cowman[3], Andrea M. Quattrini[4], Saki Harii[5], Frederic Sinniger[5], Jean-François Flot[1, 6]

Affiliations:

[1] *Evolutionary Biology and Ecology, Université libre de Bruxelles (ULB), Brussels, B-1050, Belgium.*

[2] *Systematics & Biodiversity, Justus-Liebig University, Giessen, D-35392, Germany.*

[3] *Australian Research Council (ARC) Centre of Excellence for Coral Reef Studies, James Cook University, Townsville, QLD 4811, Australia.*

[4] *Department of Invertebrate Zoology, National Museum of Natural History, Smithsonian Institution, Washington DC, 20560, USA.*

[5] *Sesoko Station, Tropical Biosphere Research Center, University of the Ryukyus, 3422 Sesoko, Motobu, Okinawa 905-0227, Japan.*

[6] *Interuniversity Institute of Bioinformatics in Brussels – (IB)2, Brussels, B-1050, Belgium.*

Corresponding authors: Catalina Ramírez-Portilla, Jean-François Flot

Emails: catalina.rzpl@gmail.com; jflot@ulb.ac.be

Abstract

Distinguishing coral species is not only crucial for physiological, ecological and evolutionary studies, but also to enable effective management of threatened reef ecosystems. However, traditional hypotheses that delineate coral species based on morphological traits from the coral skeleton are frequently at odds with tree-based molecular approaches. Additionally, a dearth of species-level molecular markers has made species delimitation particularly challenging in species-rich coral genera, leading to the widespread assumption that inter-specific hybridization might be responsible for this apparent conundrum. Here, we used three lines of evidence – morphology, breeding trials and molecular approaches – to identify species boundaries in a group of ecologically important tabular *Acropora* corals. In contrast to previous studies, our morphological analyses yielded groups that were congruent with experimental crosses as well as with coalescent-based and allele sharing-based multilocus approaches to species delimitation. Our results suggest that species of the genus *Acropora* are reproductively isolated and independently evolving units that can be distinguished morphologically. These findings not only pave the way for a taxonomic revision of coral species, but also outline an approach that can provide a solid basis to address species delimitation and provide conservation support to a wide variety of keystone organisms.

Keywords: *Acropora*, coral reefs, taxonomy, reproductive isolation, hybridization

A working coral taxonomy is crucial for meaningful physiological, ecological and population genetic studies of these keystone organisms, as well as for the effective management and conservation of the ecosystems they support (Knowlton et al. 1992; Knowlton 2001). Even though climate and anthropogenic disturbances represent substantial threats to these ecosystems (Pandolfi et al. 2003; Carpenter et al. 2008; Hughes et al. 2017, 2018a), the taxonomy and systematics of some of the most vulnerable and diverse genera remain obscure (Fukami et al. 2004b; Richards et al. 2016). Such is the case for corals of the genus *Acropora*, the species of which are among those most affected by global warming (Marshall and Baird 2000; Carpenter et al. 2008; Hughes et al. 2018b). The genus is abundant on most reefs throughout the world's tropical and sub-tropical oceans and with more than 400 nominal species it is the most diverse extant reef-building coral genus (Wallace and Willis 1994; Wallace 1999). Consequently, ascertaining species boundaries in this genus will not only advance approaches to delineate species in corals, but is also critical to understand the global response of coral reefs to climate change.

Distinguishing scleractinian coral species has always been a challenge, particularly in species-rich genera (Kitahara et al. 2016). The genus *Acropora* is emblematic of these difficulties: traditional morphological taxonomy has been mired in confusion, best highlighted by the fact that only 122 of approximately 400 nominal species were considered valid in the most recent revision of the genus (Wallace et al. 2012). Similarly, standard molecular approaches based on genetic distances or species-level monophyly have failed to delineate species. Indeed, closely related *Acropora* morphospecies usually turn out to be interspersed in

mitochondrial and nuclear gene trees (Odorico and Miller 1997; van Oppen et al. 2001; Márquez et al. 2002; Suzuki et al. 2016), which has been widely interpreted as evidence for ongoing hybridization between coral species (the "syngameon" concept; Veron 1995).

However, there are alternative interpretations of such widespread non-monophyly (Vollmer and Palumbi 2002; Funk and Omland 2003; Miller and van Oppen 2003). Polyphyletic patterns observed in gene trees can result from the incorrect identification of specimens, which is highly likely in morphologically diverse groups with an intricate taxonomy (Funk and Omland 2003). In addition, the failure of alleles to sort after speciation can produce non-monophyletic species with intraspecific distances as large as or even larger than interspecific distances (Flot et al. 2010). Such incomplete lineage sorting is more likely in species groups that have recently diversified (e.g., *Acropora* ~6 Ma; Fukami et al. 2000), as well as in species with large effective population sizes. In such cases, single-locus species delimitation approaches that require monophyly are bound to fail (Dellicour and Flot 2018).

Tabular morphospecies of *Acropora* have several features that make them an intriguing group on which to propose and validate novel taxonomic approaches (Wallace and Willis 1994): a high overall morphological similarity (Wallace 1999); the occurrence of multiple morphospecies in sympatry (Wallace 1985); and a substantial time overlap in gamete release across multiple described morphospecies (Harrison et al. 1984). *Acropora hyacinthus* (Dana 1846) is considered the epitome of tabular morphospecies and is regarded as the senior synonym for eight other nominal species (e.g., *A. bifurcata* Nemenzo 1971, *A. conferta* (Quelch 1886), *A. pectinata* (Brook 1892), *A. surculosa* (Dana 1846); Wallace 1999; Veron 2000), whereas genetic analyses suggest that it is a complex of several cryptic species (Ladner and Palumbi 2012; Suzuki et al. 2016). In addition to incongruence between molecular markers and morphological

groupings (Márquez et al. 2002; Suzuki et al. 2016), the possibility of permeable cross-breeding barriers between morphospecies (as documented in *A. hyacinthus* vs. *A. cytherea* (Dana 1846)) casts further doubts on current species boundaries (Willis et al. 1997) and makes this group an exemplar system reflecting the challenges that affect coral taxonomy as a whole.

Traditional coral taxonomy is based on features of the skeleton that can confound species delimitation due to morphological plasticity, potential homoplasy and cryptic diversity (Fukami et al. 2004b; Budd et al. 2010). However, morphology provides baseline information to identify primary species hypotheses that can be subjected to further analyses (PSHs; Puillandre et al. 2012). In addition, if evidence supports such groups as independently evolving lineages, morphological analyses can help single out characters that are taxonomically informative (Wolstenholme et al. 2003). In this study, we compared three independent lines of evidence (i.e., morphology, breeding trials and molecular approaches) to delineate species boundaries and assess hybridization in three sympatric tabular *Acropora* (Supplementary Fig. S1 available on Dryad at https://doi.org/10.5061/dryad.k98sf7m5x), inhabiting the outer reef of Sesoko Island, Okinawa, Japan (Fig. 1a).

MATERIALS AND METHODS

Colony Sampling

In the days preceding the full moon of May 2018 (29/05/2018), fragments (~8×8cm) from living tabular colonies (n=36) of reproductively mature *Acropora* (min. diameter >20cm) were collected from the outer reef (26°37'44" N, 127°51'44" E) located south of the Tropical

Biosphere Research Center (TBRC) at Sesoko Island (Okinawa, Japan). The reproductive condition of the colonies was assessed by breaking branches to expose developing oocytes (Harrison et al. 1984; Baird and Marshall 2002), and avoiding peripheral areas of the colony and tips of branches, as they usually present no gametes (Wallace 1985). Tissue samples (~2cm^3) from each colony were preserved in a guanidium thiocyanate solution (4M guanidine thiocyanate, 0.1% N-lauroylsarcosine sodium, 10mM Tris-HCl pH 8, 0.1M 2-mercaptoethanol; Fukami et al. 2004a) and alternatively in 95% ethanol for subsequent DNA extraction.

Morphological Taxonomy Assessment

Each colony was photographed in the field using an Olympus Tough TG-5 waterproof compact digital camera at the time of fragment collection (Olympus, Japan). After spawning, the fragments were bleached with a commercial solution of ~3-6% sodium hypochlorite (NaOCl) for morphometric assessment, and then stored as vouchers at the Sesoko Station (specimen photos available on Morphobank Project 4065 at http://morphobank.org/permalink/?P4065). In addition to the collected specimens, 38 tabular *Acropora* skeletons deposited in the station from other field campaigns (2015, 2019) were also used for morphometric assessment (*n*= 74 colonies in total, Dataset S1 – Morphological data available on Dryad). Qualitative and quantitative characters adapted from previous studies were recorded and measured from the coral skeletons (Supplementary Table S1 available on Dryad, see Wallace 1999; Wolstenholme et al. 2003; Wallace et al. 2012).

In order to provide a quantitative evaluation of the morphological taxonomic units (morphospecies), multivariate analyses of descriptive (qualitative) and morphometric (quantitative) characters were performed in R v3.6.2 (R Core Team 2018) through the Rstudio

console v1.2.5033 (RStudio Team 2017). Qualitative characters along with categorized quantitative variables (Supplementary Tables S1 and S2 available on Dryad) were analyzed using hierarchical clustering analysis (HCA) with simple match coefficient distances (nomclust package, v2.1.4) and the Ward clustering method (cluster package, v2.1.0, Fig. 1b). Quantitative variables with a normal distribution and homogeneity of variance (Supplementary Table S2 available on Dryad) were analyzed using linear discriminant analysis (LDA) with the maximum likelihood (ML) estimator method (MASS v 7.3-51.5 and flipMultivariates v1.0.0), and a multivariate analysis of variance (MANOVA, stats package v3.6.2) to test for significant differences (Supplementary Fig. S2a available on Dryad). Finally, using the complete morphological dataset, a factor analysis of mixed data (FAMD) was performed (FactoMineR, v2.3 and factoextra v1.0.7) to identify morphological groupings supported by all features, and to determine how much each variable contributed to the differentiation (Fig. 1c and Supplementary Fig. S2b available on Dryad). Morphospecies (groups) obtained from this morphological assessment were used as primary species hypotheses (PSHs; Puillandre et al. 2012).

Field Identification and Taxonomic Identity of the Morphospecies

Acropora bifurcata, *A. cytherea* and *A. hyacinthus* were identified in the field following Veron (2000). The main field characters for each species are as follows; *A. hyacinthus* has tapered (gradually narrowing) branches with labellate (liplike) radial corallites with a flaring lip and colonies are orange-red; *A. cytherea* has terete (cylindrical) branches with labellate radial corallites with an extended outer lip and colonies are dark brown; *A. bifurcata* has terete branches with labellate radial corallites with a square lip and colonies are light brown (see

images in Fig. 1b, color of colonies in the field and shape of radial corallites). Most local coral researchers would readily agree with the field identifications of *A. cytherea* and *A. hyacinthus*, however, *A. bifurcata* is not generally accepted as a valid species as it was considered a junior synonym of *A. hyacinthus* in the last major revision of the genus (Wallace 1999). In contrast, Veron (2000) accepted the species as valid but did not record it in Japan. However, field images in Nishihira and Veron (1995; see middle panel at p. 128) indicate that this species does occur in Japan but was identified by these authors as *A. hyacinthus*. Further information regarding type material and ongoing research into the taxonomic status of these species is presented below and summarized in Table 1.

Acropora hyacinthus (Dana 1846) has a type location in Fiji. A comparison of the colonies collected in this study to the lectotype designated by Wallace (1999, USNM 246; see http://n2t.net/ark:/65665/3fdf539df-6f98-4b91-a91c-53aa88a67457) indicates that there are significant differences in morphology. For example, the branches of the colonies at Sesoko are wider with more of a taper, which suggests that the species is distinct from that in Fiji. In consequence, the open nomenclature "aff." is used in this study to indicate that the colonies found in Sesoko have affinities with *A. hyacinthus* but belong most likely to a distinct species.

Acropora cytherea (Dana 1846) has a type location in Tahiti. A comparison of the colonies from Japan to the lectotype designated by Wallace (1999; USNM 423, see http://n2t.net/ark:/65665/367cd18b6-2f69-4451-a32b-6ae18bacd0ab) suggests that the species is morphological similar to *A. cytherea*. In particular, colonies of both species have labellate radial corallites with an extended lip. Here we used the open nomenclature qualifier "cf." to suggest that this species is possibly *A. cytherea* but further information will be required to confirm this assessment.

Acropora bifurcata Nemenzo 1971 has a type location in the Philippines. Given the proximity of Okinawa to the Philippines and the morphological similarity of the colonies to the holotype (UP C-1295, see http://www.coenomap.org/fact-sheet/acropora-bifurcata/), notably the labellate radial corallites with a squared margin, we used the open nomenclature qualifier "cf." to suggest the species is probably *A. bifurcata* but further information is required to confirm this.

Breeding Compatibility Experiments

Half of the collected colonies (*n*=18) were kept in running seawater tanks and separated in individual buckets a few hours before the predicted time of spawning. Immediately after spawning, buoyant gamete bundles containing eggs and sperm were collected at the water surface of each container for the first two colonies that spawned from each morphospecies (*n*=6). Once the eggs and sperm were separated, eggs were collected and serially washed in 0.2µm-filtered seawater to remove sperm and decrease the potential for self-fertilization. A portion of the eggs ("eggs only" – control) was kept aside in order to control for gamete separation and fertilization that may arise from leftover sperm in the eggs sample (Willis et al. 1997). The concentrated sperm obtained from the bundles was diluted approximately to 1:50 by adding filtered seawater before performing the crosses. In order to evaluate fertilization compatibility between the different morphospecies, approximately 100 washed eggs of each individual were added to each sperm dilution according to the breeding trial matrix (Fig. 2a, Dataset S2 - Breeding trials data available on Dryad).

Briefly, crosses were performed with gametes from 6 colonies for a total of *n*=6 eggs only controls and *n*=36 crosses: 6 self-control, 6 within morphospecies, and 24 between

morphospecies, with at least two replicates for each combination. The numbers of regularly shaped embryos (prawn chip stage) and unfertilized eggs were counted under a stereomicroscope approximately ten hours after the breeding trials started. Mean fertilization success (%) was calculated as the average proportion of embryos divided by the number of embryos plus the remaining unfertilized eggs (Dataset S2 - Breeding trials data available on Dryad). Non-parametric Kruskal-Wallis rank sum test (stats package v3.6.2) was performed to test for significant differences in the mean proportion fertilized, and further post-hoc tests (PMCMR v4.3 and PMCMRplus v1.4.4) were implemented in R (RStudio Team 2017; R Core Team 2018) to determine which particular crosses had significantly different fertilization success (Fig. 2b).

Preliminary Screening of Available Molecular Markers

To assess the species-level resolution of previously reported loci (Supplementary Table S3 available on Dryad), DNA was extracted from the 36 tissue samples preserved in guanidium thiocyanate solution using the NucleoSpin Tissue kit (Macherey-Nagel, Germany) and following the manufacturer's protocol. DNA integrity was assessed on agarose gels (1%) and quality checked with a NanoDrop spectrophotometer (Thermo Fisher Scientific, USA). We used the primers and protocols detailed in Supplementary Table S4 available on Dryad to perform PCR-based amplification then Sanger sequencing of the mitochondrial putative control region (AcroCR) and two nuclear exon-primed intron crossing (EPIC) markers (Ladner and Palumbi 2012): a plasma membrane calcium-transporting ATPase (PMCA) and a frizzled-4 like homolog (FZD or exon 5491). Due to the relatively short span of these markers (545 and 639 bp respectively), we re-designed primers to extend the product length of the FZD marker. For this purpose, we mapped FZD sequences previously obtained for tabular *Acropora* (Ladner and

Palumbi 2012), to the available genome assemblies (see Supplementary Table S5 available on Dryad) of *A. digitifera* (Shinzato et al. 2011), *A. millepora* (Ying et al. 2019), *A. hyacinthus* (ReFuGe 2020 Consortium 2015; Liew et al. 2016), *A. cervicornis* and *A. palmata* (Kitchen et al. 2019) using Bowtie2 v2.3.4.3 (Langmead and Salzberg 2012) in local configuration. The unambiguously mapped contigs of each genome were recovered and converted to BAM files using SAMtools v1.9 (Li et al. 2009), then transformed into BED formatted files with BEDtools v2.26.0 (Quinlan and Hall 2010). The mapped regions in the BED files were extended at least 200 bp upstream and downstream, to be then recovered from the contig FASTA files using Seqkt v1.3 (Li 2013). Alignment between the extended mapped regions and FZD original sequences was performed using Mafft (E-INS-i method; Katoh and Toh 2008).The consensus sequence for FZD (including ambiguities) was obtained from the alignment using SeaView v4.6.4 (Gouy et al. 2010) and used as target to design primers using Primer3web v4.1 (Untergasser et al. 2012), by maximizing product length and allowing for a difference of 2ºC in melting temperature between primers.

Sanger sequencing of the products was performed at GenoScreen (Lille, France). Sequencher v5.4.6 (GeneCodes, USA) was used to edit the chromatograms (Dataset 3 – Chromatograms available on Dryad). Multiple sequence alignments for each locus were generated using the E-INS-i method (Katoh and Toh 2008) in the online implementation of Mafft v7.471 (available at https://mafft.cbrc.jp/alignment/server/; Katoh et al. 2002). For the mitochondrial putative control region (AcroCR), alignments were used directly for the downstream analyses. For the sequences obtained of the EPIC markers, two different complementary phasing approaches were used. Sequences of heterozygous individuals

displaying alleles of the same length (without indel), were phased using SeqPHASE (step 1 and 2 available at https://eeg-ebe.github.io/SeqPHASE/; Flot 2010) PHASE v2.1.1 (Stephens et al. 2001; Stephens and Donnelly 2003). When length-variant heterozygotes were found in the dataset, Champuru v1.0 (Flot et al. 2006; Flot 2007) was used to phase those sequences in a first step. Subsequently, they were inputted as "known haplotype pairs" during SeqPHASE's step 1, thereby contributing to the phasing of the other individuals. Allele pairs with posterior probability ≥ 0.9 were chosen, except when more than one possible pair with similar posterior probabilities was found. In such cases, alleles shared with the highest number of individuals or that were connected with the most frequent haplotypes in the network were selected.

Model-based genetic clustering of the phased EPIC sequences was performed using STRUCTURE v2.3.4 (Pritchard et al. 2000), with admixture model, correlated allele frequencies and no prior. Implementing StrAuto v1.0 (Chhatre and Emerson 2017), values from 1 – 10 for the inferred number of populations (K) were used (20 runs per K, 250,000 burnin, 1,000,000 MCMC generations) to compute in parallel the probabilities of membership of each individual. Runs were further aligned, combined and finally merged using CLUMPP v1.1.2 (Jakobsson and Rosenberg 2007) and the Pophelper package v2.3.0 in R (Supplementary Figs. S3a and S3b available on Dryad; RStudio Team 2017; R Core Team 2018). Various species delimitation approaches were performed.

For the allele sharing-based approach (Flot et al. 2010), the EPIC markers phased sequences were input directly into the online program HaplowebMaker (available at https://eeg-ebe.github.io/HaplowebMaker/; Spöri and Flot 2020), from which haplowebs and the corresponding putative species or fields for recombination (FFRs; Doyle 1995) were obtained (Supplementary Fig. S3c available on Dryad). For the distance-based approach, the best model

of evolution was identified using the Bayesian information criterion (BIC) value criterion in ModelFinder (Kalyaanamoorthy et al. 2017). After converting the DNA alignments to bins using *fasta2DNAbin* (adegenet package v2.1.2), pairwise genetic distances using the closest available model to the best BIC score list were computed by *dist.dna* function (ape package v5.3) and histograms were plotted using ggplot2 v3.3.0.9 in R. Further phylogenetic analyses were performed under maximum likelihood (ML) with IQ-TREE v2.0.3 (Nguyen et al. 2015), using 1000 ultrafast bootstrap replicates (-B 1000) and an additional step to optimize trees by nearest neighbor interchange (-bnni; Minh et al. 2013). Branches of the consensus trees with nodes with less than 85% of bootstrap support were collapsed using *multi2di* function (ape package v5.3). Trees (Supplementary Fig. S3e available on Dryad) were visualized and formatted using FigTree v1.4.4 (Rambaut 2018). Genomic regions of *A. millepora* (Ying et al. 2019) that mapped to each nuclear loci with Bowtie2 v2.3.4.3 (--local; Langmead and Salzberg 2012), were used as outgroup for the phylogenies. For AcroCR, the closest *A. millepora* match found using megaBLAST (against the nr/nt database, available at https://blast.ncbi.nlm.nih.gov/Blast.cgi?PAGE_TYPE=BlastSearch; Altschul et al. 1990) with GenBank accession number KY408102.1 was used for that purpose instead (100% query coverage, 99.85% identity and E-value=0).

Overall, the mitochondrial AcroCR (Figs. 1d–1f) and the nuclear EPIC markers (Supplementary Fig. S3 available on Dryad) from the literature did not provide enough resolution at species-level. Model-based genetic clustering of the two EPIC markers was only able to recover two clusters (Supplementary Fig. S3a available on Dryad), neither congruent with the primary species hypotheses (PSHs) inferred from morphological species delimitation (Figs. 1b and 1c), nor with the fertilization success in breeding trials (Fig 2b). Similarly,

haplowebs obtained from these markers (Supplementary Fig. S3c available on Dryad) were not able to resolve them. Each morphospecies showed some private alleles but shared alleles connected individuals from different morphospecies into single fields for recombination (FFRs). Pairwise genetic distances and gene trees did not recover groups congruent with the other lines of evidence either (Supplementary Figs. S3d and S3e available on Dryad). For these reasons, we explored target enrichment followed by high-throughput sequencing to assess more accurately the species boundaries in this case study and to target for loci with enough resolution at species level that could be amplified in a larger dataset.

Target-Enrichment Using the Scleractinian Bait Set

To find molecular markers that provide better resolution at the species level (Supplementary Table S3), we performed target-capture sequencing for nine of the samples (*n*= 9, three from each morphospecies) preserved in 95% ethanol (Supplementary Table S6). DNA was extracted, its quality assessed and then sent to Arbor Biosciences (Ann Arbor, US) for library preparation (following Quattrini et al. 2018) and target capture sequencing (detailed in Cowman et al. 2020). For target enrichment of conserved elements (derived from exonic loci and ultraconserved elements (UCEs); Faircloth et al. 2012), we implemented a new set of baits (Cowman et al. 2020), that was re-designed from a set that originally targeted anthozoans (Quattrini et al. 2018). The new bait set targets hexacorallians (hexacoral-v2 bait set, scleractinian subset – 2,476 target loci) and has been successfully tested in a comprehensive sample of acroporids (Cowman et al. 2020). De-multiplexing, trimming, and assembly was performed according to the parameters and software previously tested in *Acropora* (Cowman et al. 2020). Subsequently, the contigs assembled for the nine tabular samples (Supplementary

Table S4) were matched to the baits employing PHYLUCE (Faircloth 2016) with default parameters (*phyluce_assembly_match_contigs_to_probes*). As a result, 2,060 loci (1,026 exons and 1,034 UCEs) were extracted into FASTA (*phyluce_assembly _get_match_counts* & *phyluce_assembly_get_fastas_from_match_counts*) to proceed with allele phasing using two different pipelines, described in the following sections (see Supplementary Table S3 available on Dryad for a summary).

Genetic Clustering and Preliminary Species Trees Using the Target-Enrichment Data Set

First, to generate a broad subset of loci that could be used to evaluate genetic clustering and estimate a preliminary species tree, loci were aligned (*phyluce_align_seqcap_align --incomplete -matrix --no-trim --aligner mafft*) and globally trimmed using Gblocks (Castresana 2000; Talavera and Castresana 2007) with default parameters (*phyluce_align_get_gblocks_trimmed_alignments_from_untrimmed*). Phasing of the aligned loci was performed following the phase_everyone v0.1 or "Laninsky" pipeline (Baca et al. 2017; Alexander 2018a). Once alleles were obtained, they were aligned and processed following steps 5 – 8 from the pipeline reference_ aligning_to_established_loci v0.0.3 (Baca et al. 2017; Alexander 2018b). Then, single nucleotide polymorphisms (SNPs) were pulled out from each loci and filtered to ensure that only loci with data for at least one individual per morphospecies were included in the downstream analyses. SNPs for the resulting 1,889 loci (1,022 exons and 867 UCEs) were used to perform a STRUCTURE analysis (Pritchard et al. 2000) parallelized through StrAuto (Chhatre and Emerson 2017), with K values from 1 – 9, admixture model, correlated allele frequencies and no prior (20 runs per K, 250,000 burnin, 1,000,000 MCMC

generations). CLUMPP (Jakobsson and Rosenberg 2007) and pophelper package tutorial (available at http://www.royfrancis.com/pophelper/articles) were used to align, combine and merge the runs. Evanno ΔK plots (Evanno et al. 2005) were used to determine the most likely number of clusters (K, Fig. 3a). Using ggplot2 v3.3.0.9 in R, the corresponding bar plots depicting the probability of individual membership to each cluster were obtained for the suggested K values (K= 3 or K=5), from which K=3 depicted better stratification of the samples according to their allele frequencies and suggested that there does not seem to be population structure within the putative species (Fig. 3b).

In addition, the most likely species tree was estimated with SNAPP v1.5.1 (Bryant et al. 2012) through the CIPRES gateway (Miller et al. 2010). SNPs were extracted from the concatenated FASTA of a subset of 210 loci present in all the samples (128 UCEs and 82 exons) using *fasta2DNAbin* (adegenet package v2.1.2) and storing them in a Nexus file using the *write.nexus.data* function (ape package v5.3). This file was used to create the XML input file in the Bayesian Evolutionary Analysis Utility (BEAUti) v2.6.3 (Bouckaert et al. 2014, 2019). Five independent runs of BEAST were performed with MCMC length of 10,000,000, pre-burnin of 100,000, sampling frequency of 1,000, and default model parameters. Output trees and log files were combined using LogCombiner v2.6.3 (Bouckaert et al. 2014, 2019). After 10% burnin, combined logs were input into Tracer v1.7.1 (Rambaut et al. 2018) to check MCMC convergence and effective sample sizes (ESS) > 200. TreeAnnotator v2.6.2 (Bouckaert et al. 2014, 2019) was used to generate maximum clade credibility trees and DensiTree v2.2.7 (Bouckaert 2010) to plot the corresponding consensus tree (Fig. 3b, left).

Estimation of a Resolved Extended Species Tree Using the Target-Enrichment Data Set

Loci were first aligned and edge trimmed (*phyluce_align_seqcap_align* --taxa 9 –incomplete-matrix) using PHYLUCE (Faircloth 2016). Subsequently, following the phasing tutorial (available at https://phyluce.readthedocs.io/en/latest/ tutorial-two.html; Andermann et al. 2019), loci were phased into alleles for each individual. Allelic sequences were aligned (*phyluce_align_seqcap_align* --no-trim –ambiguous --incomplete-matrix) and globally trimmed (*phyluce_align_get_gblocks_trimmed_alignments_from_ untrimmed*). To remove sequences with unphased bases (N) that could cause problems in downstream analyses, loci alignments were further screened and filtered (*phyluce_align_screen _alignments_for_problems*). The resulting subset of 79 loci (TC79loci hereafter) was used to perform species delimitation from the data available for the target-enriched samples. To achieve this, we estimated a resolved extended species tree using the frequency of the quartet topologies of the individual gene trees build from the phased loci alignments. However, instead of mapping individuals to species as in an extended species tree (Rabiee et al. 2019), the resulting guide tree was obtained by mapping alleles to individuals.

Similar to the preliminary screening, IQ-TREE (Nguyen et al. 2015) was implemented to obtain individual ML trees from the phased FASTA alignments obtained from the TC79loci dataset. Those trees were used as input to run ASTRAL-III v5.7.3 (Zhang et al. 2018; Rabiee et al. 2019) and to estimate a resolved extended species tree following the ASTRAL tutorial (available at https://github.com/smirarab/ASTRAL/blob/master/astral-tutorial.md#running-astral). After pruning branches with low support or local posterior probability (LPP) < 10% (Junier and Zdobnov 2010), the gene trees were used to generate a resolved extended species tree without constraining each morphospecies to be monophyletic and incorporating a mapping

file that assigned each allele sequence to an individual (-a option, Fig. 3c). Moreover, we used the same dataset to perform multi-locus species delimitation using quartet frequencies implementing SODA (Species bOundary Delimitation using Astral) v1.0.1 (Rabiee and Mirarab 2020) with the default alpha (α) threshold of 0.05 (Fig. 3c, right).

Screening for Loci with Species-Level Resolution in the Target-Enrichment Data Set

To screen for markers providing resolution at species-level, we used the mutual allelic exclusivity criterion to define species boundaries. This criterion is always met before or at the same time as reciprocal monophyly; thereby it provides a more sensitive criterion to delineate species (Flot et al. 2010). Consequently, allele sharing-based species delimitation was performed on the TC79loci dataset using both haplowebs and the corresponding conspecificity matrix (Debortoli et al. 2016) obtained using the online programs HaplowebMaker and CoMa (Spöri and Flot 2020). There, a conspecificity score (CS) was calculated for each pair of individuals by subtracting the number of markers/loci that do not support them being conspecific (H, different species or heterospecific) from the number of markers/loci for which they are considered conspecific (C, same species or partition) [*CS*= C-H]. According to these scores, the matrix was then clustered and plotted (Fig. 3d) using the R package heatmap3 v1.1.7 with the Ward agglomeration method from the *hclust* function (stats package v3.6.2). Loci with at least one individual per genetic cluster (as identified in STRUCTURE) were kept, and their corresponding haplowebs were individually explored to assess their congruence with the conspecificity matrix, and the primary species hypotheses (PSHs) inferred from the morphological assessment and supported by the breeding trials. We selected loci with haplowebs depicting partitions (FFRs) congruent with the PSHs, and that provided resolution (genetic clusters containing different

PSHs did not lump in the same FFR) even when gaps were considered as missing data. From this reduced subset, three loci with different variability degrees were chosen as candidate regions to develop markers at species level (2 exons and 1 UCE loci, Fig. 3e). GenBank megaBLAST (Altschul et al. 1990) searches were implemented (nr/nt database) to find the closest annotated match for each locus and code them accordingly (TDH, DOPR and ASNA, see Supplementary Table S7 available on Dryad).

Developing Target-Enrichment Derived Markers for Larger Datasets

To delineate species boundaries without resorting to high-throughput techniques, we used an identical approach to that previously employed to extend the length of the EPIC markers (see primer re-design performed in the section *Preliminary Screening of Available Molecular Markers* and Supplementary Table S5). From the DNA extracted of the 36 tissue samples of *Acropora* preserved in the guanidium thiocyanate solution (Fukami et al. 2004a), PCR-based amplification followed by Sanger sequencing of the three target-enrichment derived loci was performed (Supplementary Tables S3 and S4 available on Dryad). Sequences obtained from GenoScreen (Lille, France) were processed and phased as for the preliminary screened EPIC markers (PMCA and FZD).

In a first step, genetic clustering, potential population structure and admixture within the sympatric putative species was assessed using model-based genetic clustering for the derived target-capture markers (TDH, DOPR and ASNA). The corresponding ΔK plot and the bar plots to evaluate individual probability membership were performed using K =1 – 10 and the same parameters as before (Figs. 4a and 4b). Additionally, to detect clusters based on genetic

similarity and without relying in evolution models, a discriminant analysis of principal components (DAPC; Jombart et al. 2010) was completed using the package adegenet v2.1.2 in R (following Quattrini et al. 2019; Figs. 4c and 4d).

Molecular Delineation of Species Boundaries Using the Target-Enrichment Derived Markers

Among others, sampling pattern, speciation rate, species richness, mutation rate and effective population size tend to exert widely different effects and biases onto species delimitation methods (Dellicour and Flot 2018). To overcome these issues, we performed different approaches to delineate species boundaries in tabular *Acropora* study case. Distributions of pairwise genetic distances were first evaluated in search of a barcode gap (see on Dryad repository the Supplementary Fig. S4, right). As such, distance-based approaches might not work for recently diverged species, on which intraspecific distances may not be substantially smaller than interspecific ones. Consequently, we also used haplowebs and their corresponding conspecificity matrices to delineate species under the mutual allelic exclusivity criterion (Fig. 4e, Supplementary Table S8 available on Dryad). Instead of taking into account the genetic distances, such allele sharing-based approaches aggregate individuals based on the haplotypes they share, providing a more sensitive criterion to delineate closely related species (Flot et al. 2010).

To evaluate species boundaries under the reciprocal monophyly criterion, maximum likelihood phylogenies of individual (left in Supplementary Fig. S4 available on Dryad) and concatenated genes (Supplementary Fig. S5a available on Dryad) were performed on the target-capture derived loci as described for the preliminary screening of available molecular markers. Additionally, the CIPRES gateway (Miller et al. 2010) was used to perform SNAPP and

estimate the posterior distribution of trees from the SNPs extracted from the three loci. Independent runs of BEAST v2.6.3 (Bouckaert et al. 2014, 2019) were performed with MCMC length of 10,000,000, pre-burnin of 100,000, sampling frequency of 1,000, and default model parameters. After 10% burnin, the output trees and log files were combined and examined for MCMC convergence. A cloudogram depicting the most frequently recovered species trees with individuals as terminal tips (Supplementary Fig. S5b available on Dryad) was generated from this analysis. In addition, individual ML trees obtained from the phylogenetic analyses performed with IQ-TREE, were used in a resolved extended species tree estimation using ASTRAL on the three loci, both when constraining each morphospecies to be monophyletic (top left inset in Supplementary Fig. S5c available on Dryad), and without such constraint (main resolved extended species tree in Supplementary Fig. S7c available on Dryad). In both cases, alleles were mapped to individuals to obtain the final tree (using ASTRAL's -a option). Due to the small number of loci, species delimitation with SODA was not performed on this dataset.

To test for alternative species models a SNAPP coalescence-based analysis was performed (Supplementary Table S9 available on Dryad). The alternative models tested were: 1) a single species-model that includes individuals from the three morphospecies, in one complex; 2) the two species-model supported by the current taxonomy in which *A. hyacinthus* and *A. cytherea* are considered different species but *A. bifurcata* is a synonym of the former; and 3) a three species-model (*A. hyacinthus*, *A. cytherea* and *A. bifurcata*), supported by the morphological and breeding trial approaches from this study. Five runs of SNAPP were performed using BEAST, with 48 path sampling steps, 100,000 MCMC and 10,000 of pre-burnin (following Herrera and Shank 2016; Quattrini et al. 2019). Finally, ranking of the models

was performed using Bayes factor delimitation (BFD; Grummer et al. 2014; Leaché et al. 2014) by comparing the marginal likelihood estimates (MLE) obtained for each model by calculating the Bayes factor (BF; Kass and Raftery 1995) between the current taxonomy model (model 1, i.e. two accepted species) and the alternative species models (model x) , as suggested in the tutorial (BF= 2 * [model 1 - model x]; Leaché and Bouckaert 2018).

Additionally, a joint Bayesian analysis of species delimitation and species tree estimation was performed using Bayesian Phylogenetics and Phylogeography v4.2 (BPP; Yang 2015). We performed the A11-type analysis (Flouri et al. 2020), using Phylip alignments for each target-capture derived loci obtained with the *fas2phy* function of the R package chopper v0.1.8. BPP was run for 200,000 generations, with a burnin of 20,000, and a sample frequency of 1 (following McFadden et al. 2017). Comparison of replicate runs performed with each rjMCM algorithm, different starting tree topologies and initial seeds was performed to assess overall convergence. The influence of prior distributions of the ancestral population size (θ) and root age (τ_0), was evaluated under three scenarios (similar to Leaché and Fujita 2010): 1) large ancestral population size and deep divergence, 2) small ancestral population size and shallow divergence, and 3) large ancestral population size and shallow divergence among species (Supplementary Table S10 available on Dryad).

RESULTS AND DISCUSSION

Morphology Yields Primary Species Hypotheses

We first examined our collected specimens for a series of morphological characters (Tables S1, S2 and Dataset S1 available on Dryad; Wallace 1999; Wolstenholme et al. 2003;

Wallace et al. 2012). Multivariate analysis clearly distinguished three morphospecies (Figs. 1b, 1c and Supplementary Fig. S2a available on Dryad; n=74, P=<0.001), tentatively identified by comparison with the relevant type material as *A.* cf. *cytherea*, *A.* aff. *hyacinthus* and *A.* cf. *bifurcata* (see Table 1, Wallace 1999; Veron 2000; Wallace et al. 2012). The main features that contributed to the discrimination achieved by this analysis were the color of the colonies in the field, the shape and extent of crowding of the radial corallites (Fig. 1b) and the median length and width of the branches (Supplementary Fig. S2b).

Mitochondrial Marker Analyses are at Odds with Morphology

As in previous studies of the genus *Acropora* (van Oppen et al. 2001; Márquez et al. 2002), neither maximum-likelihood phylogeny (Fig. 1d) nor pairwise genetic distances (Figs. 1e and 1e) obtained from the mitochondrial putative control region (AcroCR) recovered groups congruent with the morphological analyses. Instead, specimens from the three morphospecies were scattered throughout the tree, a pattern that may result from incorrect identification of the colonies (caused for instance by morphological stasis or by phenotypic plasticity), incomplete lineage sorting or hybridization (Funk and Omland 2003).

Due to considerable overlap in the time of spawning among *Acropora* species (Harrison et al. 1984; Baird et al. 2009) and their high rates of interspecific breeding in vitro (Willis et al. 1997), hybridization has often been evoked as the most likely cause for the lack of species-level monophyly in this genus (Miller and van Oppen 2003; Willis et al. 2006). However, in groups with relatively recent diversification and significant population size, such as the *A. hyacinthus* species group (~2.58 Ma; Wallace 1999), shared ancestral polymorphisms caused by large

493 expected coalescent time should be considered as an alternative explanation. Distinguishing
494 among these competing hypotheses requires several independent markers, which is impossible
495 using only mitochondrial sequences (Sang and Zhong 2000).
496
497 *Cross-fertilization Experiments Suggest no Hybridization Potential*
498 In such situation, breeding trials not only supply an important layer of biologically
499 relevant information for delimiting sympatric species but also provide a litmus test to assess
500 hybridization potential based on *in vitro* fertilization success (Wallace and Willis 1994).
501 Consequently, we evaluated mating compatibility by performing cross-fertilization experiments
502 using representative colonies from each of the three morphospecies (Fig. 2a). Significant
503 fertilization success only occurred in crosses performed within morphospecies (Kruskal-Wallis
504 *chi-squared*= 23.26, *df* = 3, *P*= 3.565e-05), whereas all the other crosses resulted in almost no
505 fertilization (Fig. 2b). The reproductively isolated groups delineated using this approach
506 comprised only individuals of the same morphospecies, thereby supporting the boundaries
507 inferred from morphology.
508
509 *Molecular Evidence Supports the Primary Species Hypotheses*
510 Since breeding compatibility experiments can only be performed between colonies that
511 reproduce synchronously or within a few hours of difference (Willis et al. 1997), we extended
512 the scope of the cross-fertilization trials by looking at patterns of genetic clustering and allele
513 sharing, i.e. using genetic similarity and mutual allelic exclusivity as indirect evidence for
514 reproductive isolation (Supplementary Table S3). Molecular approaches stemming from high-
515 throughput techniques have recently overcome long-standing methodological limitations of

molecular studies such as the small number of markers available and lack of species-level resolution (Cowman et al. 2020; Erickson et al. 2021). Here, three individuals per morphospecies (*n*=9) were analyzed applying an enrichment procedure designed to capture conserved elements (derived from UCEs and exonic loci) with a set of baits targeting hexacorals (Quattrini et al. 2018; Cowman et al. 2020). Using this approach, more than two thousand phased loci were recovered (1,026 exons and 1,034 UCEs, Supplementary Table S6).

Model-based genetic clustering using STRUCTURE (Figs. 3a and 3b), as well as an ASTRAL resolved extended species tree (Fig. 3c) of subsets of these loci (1889 and 79 loci respectively), identified groups that were consistent with both morphology and breeding trials. To verify this across a larger number of specimens, we screened the captured loci for candidate markers displaying allelic exclusivity for each cluster (79 loci, Fig. 3d). As a result, three nuclear loci – L-threonine 3-dehydrogenase (TDH), dopamine receptor 2 (DOPR) and ATPase ASNA-1 (ASNA) (Fig. 3e) – were selected for PCR-based amplification of the 36 individuals in the tabular *Acropora* dataset followed by various molecular species delimitation approaches (Supplementary Tables S3, S4 and S7).

Genetic clustering of the specimens (*n*=36) differentiated three groups that were congruent with both morphospecies hypotheses and breeding compatibility results (Figs. 4a-4d). As previously observed with the mitochondrial control region, the pairwise genetic distances between and within morphospecies overlapped for each marker (Supplementary Fig. S4, right), and neither the individual gene phylogenies (Supplementary Fig. S4, left), a concatenated tree (Supplementary Fig. S5a) nor a cloudogram (Supplementary Fig. S5b) inferred from these loci supported the reciprocal monophyly of the three species.

538 By contrast, each of the three species was recovered as monophyletic in the resolved
539 extended species tree obtained using ASTRAL (Supplementary Fig. S5c), albeit with uncertain
540 topology and low support for some clades. In addition, the haplowebs inferred from these three
541 loci (Fig. 4e) and the conspecificity matrix summarizing them (Fig. 4f and Supplementary Table
542 S8) all unequivocally supported the grouping of our samples into three reproductively isolated
543 units. Similarly, coalescence-based (Supplementary Table S9) and Bayesian species delimitation
544 analyses (Supplementary Table S10) supported the three-species model with decisive values
545 (Bayes factor >10 and posterior probability > 0.95, respectively).
546 These results challenge the generally accepted idea that morphospecies of *Acropora*
547 cannot be distinguished using molecular approaches because of hybridization. On the contrary,
548 despite being closely related these species appear to be reproductively isolated. It was possible to
549 delineate them using target-enrichment followed by genomic sequencing (which probes
550 thousands of markers but can yield incomplete data matrices) as well as using traditional PCR
551 amplification followed by Sanger sequencing (which targets only one marker/individual at a
552 time but yields high-quality, complete datasets). Hence, our results are different from other
553 examples of successful molecular species delimitation based exclusively on high-throughput
554 genomic sequencing (Quattrini et al. 2019; Erickson et al. 2021).
555
556 *Conclusions*
557 By using approaches sensitive enough to detect divergence at both the morphological and
558 molecular levels, congruence between the three lines of evidence (i.e., morphology, breeding
559 trials, and molecular approaches) demonstrates that it is possible to develop a robust coral
560 taxonomy, thus helping to solve one of the greatest taxonomical conundrums since Linnaeus

(Kitahara et al. 2016). Comparing evidence from multiple independent sources improved confidence in coral species boundaries by illustrating that *Acropora* species, once considered a taxonomic nightmare, are actually reproductively isolated and independently evolving units that can be distinguished morphologically.

Our findings show that allele sharing-based and coalescence-based multilocus approaches to species delimitation outperform mainstream methodologies relying on monophyly and genetic distance as the criteria to delineate boundaries, particularly between closely related species. Although our methodology was focused on the taxonomic revision of coral species, the approaches outlined here are in principle applicable to a wide variety of plant and animal taxa.

SUPPLEMENTARY MATERIAL

The main sequence datasets generated for this study have been placed in GenBank and SRA repositories (see Supplementary Tables S4 and S5 available in Dryad). All photographical records of the specimens used for this study have been deposited in MorphoBank (Project 4065, http://morphobank.org/permalink/?P4065). Alignments, trees and examples of scripts and commands used can be found in the GitHub repository (https://github.com/catalinarp/SpeciesDelimitationTabularAcropora). All other supplementary files and materials are available in the Dryad repository (https://doi.org/10.5061/dryad.k98sf7m5x).

FUNDING

This work was partially supported by the Collaborative Research of the Tropical Biosphere Research Center – TBRC, University of the Ryukyus to A.H.B. C.R.P. was supported by the Fonds de la Recherche Scientifique – FNRS via an "ASP" PhD fellowship (n° 1.A.835.18F) as well as travel grants, and Fonds David et Alice Van Buuren (Fondattion Jaumotte-Demoulin). A.H.B. & P.F.C. were funded by the Australian Research Council – ARC Centre of Excellence for Coral Reef Studies (Programme CE140100020), the ARC Discovery Early Career Researcher Award – DECRA Fellowship (DE170100516 to P.F.C) and the Japan Society for the Promotion of Science – JSPS Short Term Fellowship (S-15086 to A.H.B). J.-F.F. was supported by the Fonds de la Recherche Scientifique – FNRS under CDR Grant n°J.0272.17 and by the Fédération Wallonie-Bruxelles via an ARC grant.

ACKNOWLEDGMENTS

The assistance provided in the field by B. Lust, T. I. Terraneo and our colleagues at the Sesoko Station (TBRC) was greatly appreciated. We are grateful to O. Hardy, M. Kochzius and T. Wilke for useful discussions regarding this study. Furthermore, we want to thank S. Dellicour, A. F. Sands, B. A. Dayrat (Associate Editor) and two anonymous reviewers for their insightful comments on the manuscript. We acknowledge the computational resources provided by the Consortium des Équipements de Calcul Intensif (CÉCI). Sample collection was performed under Okinawa Prefecture permits: No. 27-28 (2015), No. 30-25 (2018) and No. 31-26 (2019).

REFERENCES

Alexander A. 2018a. phase_everyone v0.1. Available from https://github.com/laninsky/reference_aligning_to_established_loci/edit/master/phase_every

605 one.
606 Alexander A. 2018b. Reference_aligning_to_established_loci v0.0.3. Available from
607 https://github.com/laninsky/reference_aligning_to_established_loci.
608 Altschul S.F.S.F., Gish W., Miller W., Myers E.W.E.W., Lipman D.J.D.J. 1990. Basic local
609 alignment search tool. J. Mol. Biol. 215:403–410.
610 Andermann T., Fernandes A.M., Olsson U., Töpel M., Pfeil B., Oxelman B., Aleixo A., Faircloth
611 B.C., Antonelli A. 2019. Allele phasing greatly improves the phylogenetic utility of
612 Ultraconserved Elements. Syst. Biol. 68:32–46.
613 Baca S.M., Alexander A., Gustafson G.T., Short A.E.Z. 2017. Ultraconserved elements show
614 utility in phylogenetic inference of Adephaga (Coleoptera) and suggest paraphyly of
615 'Hydradephaga.' Syst. Entomol. 42:786–795.
616 Baird A.H., Guest J.R., Willis B.L. 2009. Systematic and biogeographical patterns in the
617 reproductive biology of scleractinian corals. Annu. Rev. Ecol. Evol. Syst. 40:551–571.
618 Baird A.H., Marshall P.A. 2002. Mortality, growth and reproduction in scleractinian corals
619 following bleaching on the Great Barrier Reef. Mar. Ecol. Prog. Ser. 237:133–141.
620 Bouckaert R., Heled J., Kühnert D., Vaughan T., Wu C.H., Xie D., Suchard M.A., Rambaut A.,
621 Drummond A.J. 2014. BEAST 2: A Software Platform for Bayesian Evolutionary Analysis.
622 PLoS Comput. Biol. 10:1–6.
623 Bouckaert R., Vaughan T.G., Barido-Sottani J., Duchêne S., Fourment M., Gavryushkina A.,
624 Heled J., Jones G., Kühnert D., De Maio N., Matschiner M., Mendes F.K., Müller N.F.,
625 Ogilvie H.A., Du Plessis L., Popinga A., Rambaut A., Rasmussen D., Siveroni I., Suchard
626 M.A., Wu C.H., Xie D., Zhang C., Stadler T., Drummond A.J. 2019. BEAST 2.5: An

advanced software platform for Bayesian evolutionary analysis. PLoS Comput. Biol. 15:1–28.

Bouckaert R.R. 2010. DensiTree: Making sense of sets of phylogenetic trees. Bioinformatics. 26:1372–1373.

Brook G. 1892. Preliminary descriptions of new species of *Madrepora* in the collections of the British Museum. Part II. Ann. Mag. Nat. Hist. 10:451–465.

Bryant D., Bouckaert R., Felsenstein J., Rosenberg N.A., Roychoudhury A. 2012. Inferring species trees directly from biallelic genetic markers: bypassing gene trees in a full coalescent analysis. Mol. Biol. Evol. 29:1917–1932.

Budd A.F., Romano S.L., Smith N.D., Barbeitos M.S. 2010. Rethinking the phylogeny of scleractinian corals: a review of morphological and molecular data. Integr. Comp. Biol. 50:411–427.

Carpenter K.E., Abrar M., Aeby G., Aronson R.B., Banks S., Bruckner A., Chiriboga A., Cortés J., Delbeek J.C., DeVantier L., Edgar G.J., Edwards A.J., Fenner D., Guzmán H.M., Hoeksema B.W., Hodgson G., Johan O., Licuanan W.Y., Livingstone S.R., Lovell E.R., Moore J.A., Obura D.O., Ochavillo D., Polidoro B.A., Precht W.F., Quibilan M.C., Reboton C., Richards Z.T., Rogers A.D., Sanciangco J., Sheppard A., Sheppard C., Smith J., Stuart S., Turak E., Veron J.E.N., Wallace C., Weil E., Wood E. 2008. One-third of reef-building corals face elevated extinction risk from climate change and local impacts. Science. 321:560–563.

Castresana J. 2000. Selection of conserved blocks from multiple alignments for their use in phylogenetic analysis. Mol. Biol. Evol. 17:540–552.

Chhatre V.E., Emerson K.J. 2017. StrAuto: Automation and parallelization of STRUCTURE

650 analysis. BMC Bioinformatics. 18:1–5.
651 Cowman P.F., Quattrini A.M., Bridge T.C., Watkins-Colwell G.J., Fadli N., Grinblat M., Roberts
652 T.E., McFadden C.S., Miller D.J., Baird A.H. 2020. An enhanced target-enrichment bait set
653 for Hexacorallia provides phylogenomic resolution of the staghorn corals (Acroporidae) and
654 close relatives. Mol. Phylogenetics Evol. 153:106944.
655 Dana J.D. 1846. Zoophytes. United States Exploring Expedition during the years 1838-1842.
656 Philadelphia: Lea and Blanchard. p. 740.
657 Debortoli N., Li X., Eyres I., Fontaneto D., Hespeels B., Tang C.Q., Flot J.-F.F., Van Doninck K.
658 2016. Genetic exchange among bdelloid rotifers is more likely due to horizontal gene
659 transfer than to meiotic sex. Curr. Biol. 26:723–732.
660 Dellicour S., Flot J.F. 2018. The hitchhiker's guide to single-locus species delimitation. Mol.
661 Ecol. Resour. 18:1234–1246.
662 Doyle J.J. 1995. The irrelevance of allele tree topologies for species delimitation, and a non-
663 topological alternative. Syst. Bot. 20:574–588.
664 Erickson K.L., Pentico A., Quattrini A.M., McFadden C.S. 2021. New approaches to species
665 delimitation and population structure of anthozoans: Two case studies of octocorals using
666 ultraconserved elements and exons. Mol. Ecol. Resour. 21:78–92.
667 Evanno G., Regnaut S., Goudet J. 2005. Detecting the number of clusters of individuals using the
668 software STRUCTURE: A simulation study. Mol. Ecol. 14:2611–2620.
669 Faircloth B.C. 2016. PHYLUCE is a software package for the analysis of conserved genomic
670 loci. Bioinformatics. 32:786–788.
671 Faircloth B.C., McCormack J.E., Crawford N.G., Harvey M.G., Brumfield R.T., Glenn T.C.

2012. Ultraconserved elements anchor thousands of genetic markers spanning multiple evolutionary timescales. Syst. Biol. 61:717–726.

Flot J.-F. 2010. Seqphase: A web tool for interconverting phase input/output files and fasta sequence alignments. Mol. Ecol. Resour. 10:162–166.

Flot J.-F., Couloux A., Tillier S. 2010. Haplowebs as a graphical tool for delimiting species: a revival of Doyle's "field for recombination" approach and its application to the coral genus *Pocillopora* in Clipperton. BMC Evol. Biol. 10:372.

Flot J.F. 2007. Champuru 1.0: A computer software for unraveling mixtures of two DNA sequences of unequal lengths. Mol. Ecol. Notes. 7:974–977.

Flot J.F., Tillier A., Samadi S., Tillier S. 2006. Phase determination from direct sequencing of length-variable DNA regions. Mol. Ecol. Notes. 6:627–630.

Flouri T., Rannala B., Yang Z. 2020. A tutorial on the use of BPP for species tree estimation and species delimitation. In: Scornavacca C., Delsuc F., Galtier N., editors. Phylogenetics in the genomic era. HAL archives-ouvertes. p. 5.6:1–5.6:16.

Fukami H., Budd A.F., Levitan D.R., Jara J., Kersanach R., Knowlton N. 2004a. Geographic differences in species boundaries among members of the *Montastraea annularis* complex based on molecular and morphological markers. Evolution. 58:324–337.

Fukami H., Budd A.F., Paulay G., Solé-Cava A., Chen C.A., Iwao K., Knowlton N. 2004b. Conventional taxonomy obscures deep divergence between Pacific and Atlantic corals. Nature. 427:832–835.

Fukami H., Omori M., Hatta M. 2000. Phylogenetic relationships in the coral family Acroporidae, reassessed by inference from mitochondrial genes. Zoolog. Sci. 17:689–696.

Funk D.J., Omland K.E. 2003. Species-level paraphyly and polyphyly: frequency, causes, and

695 consequences, with insights from animal mitochondrial DNA. Annu. Rev. Ecol. Evol. Syst.
696 34:397–423.
697 Gouy M., Guindon S., Gascuel O. 2010. SeaView version 4: A multiplatform graphical user
698 interface for sequence alignment and phylogenetic tree building. Mol. Biol. Evol. 27:221–
699 224.
700 Grummer J.A., Bryson R.W., Reeder T.W. 2014. Species delimitation using Bayes factors:
701 Simulations and application to the *Sceloporus scalaris* species group (Squamata:
702 Phrynosomatidae). Syst. Biol. 63:119–133.
703 Harrison P.L., Babcock R.C., Bull G.D., Oliver J.K., Wallace C.C., Willis B.L. 1984. Mass
704 spawning in tropical reef corals. Science. 223:1186–1189.
705 Herrera S., Shank T.M. 2016. RAD sequencing enables unprecedented phylogenetic resolution
706 and objective species delimitation in recalcitrant divergent taxa. Mol. Phylogenetics Evol.
707 100:70–79.
708 Hughes T.P., Anderson K.D., Connolly S.R., Heron S.F., Kerry J.T., Lough J.M., Baird A.H.,
709 Baum J.K., Berumen M.L., Bridge T.C., Claar D.C., Eakin C.M., Gilmour J.P., Graham
710 N.A.J., Harrison H., Hobbs J.P.A., Hoey A.S., Hoogenboom M., Lowe R.J., McCulloch
711 M.T., Pandolfi J.M., Pratchett M., Schoepf V., Torda G., Wilson S.K. 2018a. Spatial and
712 temporal patterns of mass bleaching of corals in the Anthropocene. Science. 359:80–83.
713 Hughes T.P., Barnes M.L., Bellwood D.R., Cinner J.E., Cumming G.S., Jackson J.B.C., Kleypas
714 J., Van De Leemput I.A., Lough J.M., Morrison T.H., Palumbi S.R., Van Nes E.H.,
715 Scheffer M. 2017. Coral reefs in the Anthropocene. Nature. 546:82–90.
716 Hughes T.P., Kerry J.T., Baird A.H., Connolly S.R., Dietzel A., Eakin C.M., Heron S.F., Hoey

A.S., Hoogenboom M.O., Liu G., McWilliam M.J., Pears R.J., Pratchett M.S., Skirving W.J., Stella J.S., Torda G. 2018b. Global warming transforms coral reef assemblages. Nature. 556:492–496.

Jakobsson M., Rosenberg N.A. 2007. CLUMPP: A cluster matching and permutation program for dealing with label switching and multimodality in analysis of population structure. Bioinformatics. 23:1801–1806.

Jombart T., Devillard S., Balloux F. 2010. Discriminant analysis of principal components: a new method for the analysis of genetically structured populations. BMC Genet. 11:94.

Junier T., Zdobnov E.M. 2010. The Newick utilities: high-throughput phylogenetic tree processing in the UNIX shell. Bioinformatics. 26:1669–1670.

Kalyaanamoorthy S., Minh B.Q., Wong T.K.F., Von Haeseler A., Jermiin L.S. 2017. ModelFinder: Fast model selection for accurate phylogenetic estimates. Nat. Methods. 14:587–589.

Kass R.E., Raftery A.E. 1995. Bayes factors. J. Am. Stat. Assoc. 90:773–795.

Katoh K., Misawa K., Kuma K.I., Miyata T. 2002. MAFFT: A novel method for rapid multiple sequence alignment based on fast Fourier transform. Nucleic Acids Res. 30:3059–3066.

Katoh K., Toh H. 2008. Recent developments in the MAFFT multiple sequence alignment program. Brief. Bioinform. 9:286–298.

Kitahara M. V., Fukami H., Benzoni F., Huang D. 2016. The new systematics of Scleractinia: integrating molecular and morphological evidence. In: S. G., Z. D., editors. The Cnidaria, Past, Present and Future. Cham: Springer. p. 41–59.

Kitchen S.A., Ratan A., Bedoya-Reina O.C., Burhans R., Fogarty N.D., Miller W., Baums I.B. 2019. Genomic variants among threatened *Acropora* corals. G3 Genes, Genomes, Genet.

9:1633–1646.

Knowlton N. 2001. Who are the players on coral reefs and does it matter? The importance of coral taxonomy for coral reef management. Bull. Mar. Sci. 69:305–308.

Knowlton N., Weil E., Weight L.A., Guzman H.M. 1992. Sibling species in *Montastraea annularis*, coral bleaching, and the coral climate record. Science. 255:330–333.

Ladner J.T., Palumbi S.R. 2012. Extensive sympatry, cryptic diversity and introgression throughout the geographic distribution of two coral species complexes. Mol. Ecol. 21:2224–2238.

Langmead B., Salzberg S.L. 2012. Fast gapped-read alignment with Bowtie 2. Nat. Methods. 9:357–359.

Leaché A.D., Bouckaert R.R. 2018. Species trees and species delimitation with SNAPP: a tutorial and worked example version. Work. Popul. Speciat. genomics.:1–17.

Leaché A.D., Fujita M.K. 2010. Bayesian species delimitation in West African forest geckos (*Hemidactylus fasciatus*). Proc. R. Soc. B Biol. Sci. 277:3071–3077.

Leaché A.D., Fujita M.K., Minin V.N., Bouckaert R.R. 2014. Species delimitation using genome-wide SNP Data. Syst. Biol. 63:534–542.

Li H. 2013. Seqtk: a fast and lightweight tool for processing FASTA or FASTQ sequences. .

Li H., Handsaker B., Wysoker A., Fennell T., Ruan J., Homer N., Marth G., Abecasis G., Durbin R. 2009. The Sequence Alignment/Map format and SAMtools. Bioinformatics. 25:2078–2079.

Liew Y.J., Aranda M., Voolstra C.R. 2016. Reefgenomics.Org – a repository for marine genomics data. Database.

Márquez L.M., Van Oppen M.J.H., Willis B.L., Reyes A., Miller D.J. 2002. The highly cross-fertile coral species, *Acropora hyacinthus* and *Acropora cytherea*, constitute statistically distinguishable lineages. Mol. Ecol. 11:1339–1349.

Marshall P.A., Baird A.H. 2000. Bleaching of corals on the Great Barrier Reef: differential susceptibilities among taxa. Coral Reefs. 19:155–163.

McFadden C.S., Haverkort-Yeh R., Reynolds A.M., Halàsz A., Quattrini A.M., Forsman Z.H., Benayahu Y., Toonen R.J. 2017. Species boundaries in the absence of morphological, ecological or geographical differentiation in the Red Sea octocoral genus *Ovabunda* (Alcyonacea: Xeniidae). Mol. Phylogenet. Evol. 112:174–184.

Miller D.J., van Oppen M.J.H. 2003. A 'fair go' for coral hybridization. Mol. Ecol. 12:805–807.

Miller M.A., Pfeiffer W., Schwartz T. 2010. Creating the CIPRES Science Gateway for inference of large phylogenetic trees. 2010 Gatew. Comput. Environ. Work. GCE 2010.

Minh B.Q., Nguyen M.A.T., Von Haeseler A. 2013. Ultrafast approximation for phylogenetic bootstrap. Mol. Biol. Evol. 30:1188–1195.

Nemenzo F. 1971. Systematic studies on Philippine shallow-water scleractinians: VII. Additional forms. Nat. Appl. Sci. Bull. Univ. Philipp. 23:141–209.

Nguyen L.T., Schmidt H.A., Von Haeseler A., Minh B.Q. 2015. IQ-TREE: A fast and effective stochastic algorithm for estimating maximum-likelihood phylogenies. Mol. Biol. Evol. 32:268–274.

Nishihira M., Veron J.E.N. 1995. Hermatypic corals of Japan. Tokyo: Kaiyusha.

Odorico D.M., Miller D.J. 1997. Variation in the ribosomal internal transcribed spacers and 5.8S rDNA among five species of Acropora (Cnidaria; Scleractinia): Patterns of variation consistent with reticulate evolution. Mol. Biol. Evol. 14:465–473.

van Oppen M.J.H., McDonald B.J., Willis B., Miller D.J. 2001. The evolutionary history of the coral genus *Acropora* (Scleractinia, Cnidaria) based on a mitochondrial and a nuclear marker: reticulation, incomplete lineage sorting, or morphological convergence? Mol. Biol. Evol. 18:1315–1329.

Pandolfi J.M., Bradbury R.H., Sala E., Hughes T.P., Bjorndal K.A., Cooke R.G., McArdle D., McClenachan L., Newman J.H. M., Paredes G., Warner R.R., Jackson J.B.C. 2003. Global trajectories of the long-term decline of coral reef ecosystem. Science. 301:955–958.

Pritchard J.K., Stephens M., Donnelly P. 2000. Inference of population structure using multilocus genotype data. Genetics. 155:945–959.

Puillandre N., Modica M. V., Zhang Y., Sirovich L., Boisselier M.C., Cruaud C., Holford M., Samadi S. 2012. Large-scale species delimitation method for hyperdiverse groups. Mol. Ecol. 21:2671–2691.

Quattrini A.M., Faircloth B.C., Dueñas L.F., Bridge T.C.L., Brugler M.R., Calixto-Botía I.F., DeLeo D.M., Forêt S., Herrera S., Lee S.M.Y., Miller D.J., Prada C., Rádis-Baptista G., Ramírez-Portilla C., Sánchez J.A., Rodríguez E., McFadden C.S. 2018. Universal target-enrichment baits for anthozoan (Cnidaria) phylogenomics: New approaches to long-standing problems. Mol. Ecol. Resour. 18:281–295.

Quattrini A.M., Wu T., Soong K., Jeng M.S., Benayahu Y., McFadden C.S. 2019. A next generation approach to species delimitation reveals the role of hybridization in a cryptic species complex of corals. BMC Evol. Biol. 19:1–19.

Quelch J.J. 1886. Report on the Reef-corals collected by H.M.S. Challenger during the years 1873–1876. Zoology. 16:1–203.

807 Quinlan A.R., Hall I.M. 2010. BEDTools: A flexible suite of utilities for comparing genomic
808 features. Bioinformatics. 26:841–842.
809 R Core Team. 2018. R: A language and environment for statistical computing. .
810 Rabiee M., Mirarab S. 2020. SODA: Multi-locus species delimitation using quartet frequencies.
811 Bioinformatics. 36:5623–5631.
812 Rabiee M., Sayyari E., Mirarab S. 2019. Multi-allele species reconstruction using ASTRAL.
813 Mol. Phylogenet. Evol. 130:286–296.
814 Rambaut A. 2018. FigTree: a graphical viewer of phylogenetic trees. Available from
815 http://tree.bio.ed.ac.uk/software/figtree/.
816 Rambaut A., Drummond A.J., Xie D., Baele G., Suchard M.A. 2018. Posterior summarization in
817 Bayesian phylogenetics using Tracer 1.7. Syst. Biol. 67:901–904.
818 ReFuGe 2020 Consortium. 2015. The ReFuGe 2020 Consortium – using "omics" approaches to
819 explore the adaptability and resilience of coral holobionts to environmental change. Front.
820 Mar. Sci. 2:68.
821 Richards Z.T., Berry O., van Oppen M.J.H. 2016. Cryptic genetic divergence within threatened
822 species of *Acropora* coral from the Indian and Pacific Oceans. Conserv. Genet. 17:577–591.
823 RStudio Team. 2017. RStudio: Integrated development for R. .
824 Sang T., Zhong Y. 2000. Testing hybridization hypotheses based on incongruent gene trees.
825 Syst. Biol. 49:422–434.
826 Shinzato C., Shoguchi E., Kawashima T., Hamada M., Hisata K., Tanaka M., Fujie M., Fujiwara
827 M., Koyanagi R., Ikuta T., Fujiyama A., Miller D.J., Satoh N. 2011. Using the *Acropora*
828 *digitifera* genome to understand coral responses to environmental change. Nature. 476:320–
829 323.

Spöri Y., Flot J.-F. 2020. HaplowebMaker and CoMa: two web tools to delimit species using haplowebs and conspecificity matrices. Methods Ecol. Evol. 11:1434–1438.

Stephens M., Donnelly P. 2003. A comparison of bayesian methods for haplotype reconstruction from population genotype data. Am. J. Hum. Genet. 73:1162–1169.

Stephens M., Smith N.J., Donnelly P. 2001. A new statistical method for haplotype reconstruction from population data. Am. J. Hum. Genet. 68:978–989.

Suzuki G., Keshavmurthy S., Hayashibara T., Wallace C.C., Shirayama Y., Chen C.A., Fukami H. 2016. Genetic evidence of peripheral isolation and low diversity in marginal populations of the *Acropora hyacinthus* complex. Coral Reefs. 35:1419–1432.

Talavera G., Castresana J. 2007. Improvement of phylogenies after removing divergent and ambiguously aligned blocks from protein sequence alignments. Syst. Biol. 56:564–577.

Untergasser A., Cutcutache I., Koressaar T., Ye J., Faircloth B.C., Remm M., Rozen S.G. 2012. Primer3 - New capabilities and interfaces. Nucleic Acids Res. 40:1–12.

Veron J.E.N. 1995. Corals in space and time: the biogeography and evolution of the Scleractinia. Ithaca, NY: Cornell University Press.

Veron J.E.N. 2000. Corals of the World. Townsville: Australian Institute of Marine Science (AIMS).

Vollmer S. V, Palumbi S.R. 2002. Hybridization and the evolution of reef coral diversity. Science. 296:2023–2025.

Wallace C. 1999. Staghorn corals of the world: a revision of the genus *Acropora*. Collibgwood, Victoria: CSIRO Publishing.

Wallace C.C. 1985. Reproduction, recruitment and fragmentation in nine sympatric species of

852 the coral genus *Acropora*. Mar. Biol. 88:217–233.
853 Wallace C.C., Done B.J., Muir P.R. 2012. Revision and catalogue of worldwide staghorn corals
854 *Acropora* and *Isopora* (Scleractinia: Acroporidae) in the Museum of Tropical Queensland.
855 Mem. Queensl. Museum. 52:1–22.
856 Wallace C.C., Willis B.L. 1994. Systematics of the coral genus *Acropora*: implications of new
857 biological findings for species concepts. Annu. Rev. Ecol. Syst. 25:237–262.
858 Willis B.L., Babcock R.C., Harrison P.L., Wallace C.C. 1997. Experimental hybridization and
859 breeding incompatibilities within the mating systems of mass spawning reef corals. Coral
860 Reefs. 16:S53–S65.
861 Willis B.L., van Oppen M.J.H., Miller D.J., Vollmer S. V, Ayre D.J. 2006. The role of
862 hybridization in the evolution of reef corals. Annu. Rev. Ecol. Evol. Syst. 37:489–517.
863 Wolstenholme J.K., Wallace C.C., Chen C.A. 2003. Species boundaries within the *Acropora*
864 *humilis* species group (Cnidaria; Scleractinia): a morphological and molecular interpretation
865 of evolution. Coral Reefs. 22:155–166.
866 Yang Z. 2015. The BPP program for species tree estimation and species delimitation. Curr. Zool.
867 61:854–865.
868 Ying H., Hayward D.C., Cooke I., Wang W., Moya A., Siemering K.R., Sprungala S., Ball E.E.,
869 Forêt S., Miller D.J. 2019. The whole-genome sequence of the coral *Acropora millepora*.
870 Genome Biol. Evol. 11:1374–1379.
871 Zhang C., Rabiee M., Sayyari E., Mirarab S. 2018. ASTRAL-III: Polynomial time species tree
872 reconstruction from partially resolved gene trees. BMC Bioinformatics. 19:15–30.
873

874

875 FIGURE CAPTIONS

876

877 FIGURE 1. Morphology yields primary species hypotheses that are at odds with the mitochondrial
878 phylogeny. a) Tabular *Acropora* at Sesoko Island outer reef (Okinawa, Japan); photo by A.H.
879 Baird). b) Hierarchical clustering analysis (HCA, agglomerative coefficient= 0.95), along with
880 the main morphological features that contributed to the differentiation for each morphospecies:
881 color of colonies in the field (left) and shape and crowding of radial corallites along branches
882 (right). c) Factor analysis of mixed data (FAMD) based on both qualitative and quantitative
883 characters, distinguishing three morphospecies: *A.* cf. *bifurcata*, *A.* cf. *cytherea* and *A.* aff.
884 *hyacinthus*. See also Figure S2 and Table S1 for additional information. d) Maximum likelihood
885 (ML) phylogeny of the mitochondrial control region (AcroCR) using ultrafast bootstrap.
886 Branches with less than 85% of bootstrap support (BS) were collapsed. e) Haplotype network of
887 the AcroCR region shaded according to morphospecies, with gaps recoded as single base
888 changes. f) Histogram of the pairwise genetic distances of the AcroCR sequences within and
889 between morphospecies.

890

891 FIGURE 2. Cross-fertilization experiments suggest no hybridization potential. a) Gamete
892 combinations (sperm x eggs) performed between representative colonies of each tabular
893 *Acropora* morphospecies. b) Fertilization success (%) in each category of breeding trial,
894 including the "eggs only" [top cells with bold border in a)] and the "self" fertilization controls

895 [diagonal cells with bold font in a)] to account for sperm contamination and potential self-
896 compatibility respectively.
897
898 FIGURE 3. Screening of target capture-derived markers. a) Evanno ΔK plot (above) depicting two
899 possible optimal cluster (K) values (dashed lines) and bar plots (below) displaying the individual
900 probability of membership assigned using model-based clustering for each K value (1889 loci).
901 The most frequent SNAPP tree (using 210 loci present in all samples) is depicted on the left side
902 of the plots. b) ASTRAL resolved extended species tree with phased sequences color-coded
903 according to the molecular species delineated by SODA, where alleles were mapped to
904 individuals and nodes with less than 10% of local posterior probability (LPP) or low branch
905 support were collapsed. c) Conspecificity score (CS) matrix for a subset of 79 target-enrichment
906 sequenced loci used to perform a preliminary allele sharing-based species delimitation. d)
907 Haplowebs of three loci displaying putative species delimitation under mutual allelic exclusivity
908 criterion, congruent with model-based genetic clustering, species trees and the primary species
909 hypotheses (PSHs) based on morphology and breeding trials.
910
911 FIGURE 4. Molecular evidence supports the primary species hypotheses in *Acropora* corals. a)
912 Evanno ΔK plot highlighting the most likely number of genetic clusters in red. b) Bayesian
913 model-based genetic structure plot depicting the probability of individual membership to each
914 cluster when K=3. c) Optimal cluster number for the Discriminant analysis of principal
915 components (DAPC) according to the Bayesian Information Criterion (BIC) statistic with the
916 most likely K value highlighted in red (K=3). d) DAPC scatterplot depicting clustering based on
917 genetic similarity among the individuals using two discriminant functions (DF). e) Haplowebs

delineating putative species based on the co-occurrence of alleles for each one of the nuclear markers defined from target-capture sequencing, color-coded according to morphospecies. f) Conspecificity score (CS) matrix summarizing the fields for recombination (FFRs) found using the allele sharing-based approach to delineate species with the three target-capture defined loci. The conspecific groups delineated by the FFRs of the three markers are congruent with the morphospecies and with the results from breeding trials (see Figs. 1 and 2).

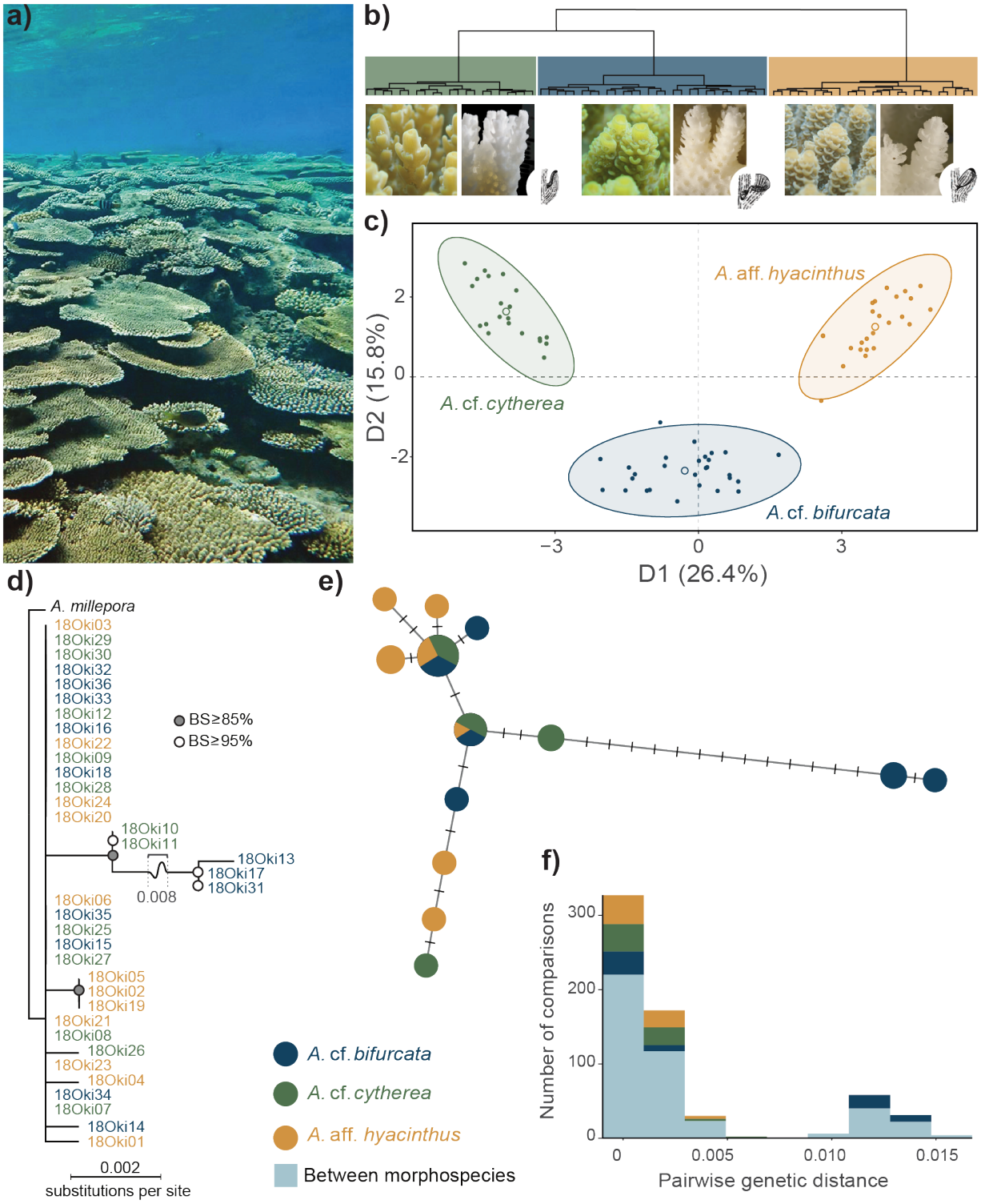

925

926 FIGURE 1.

927

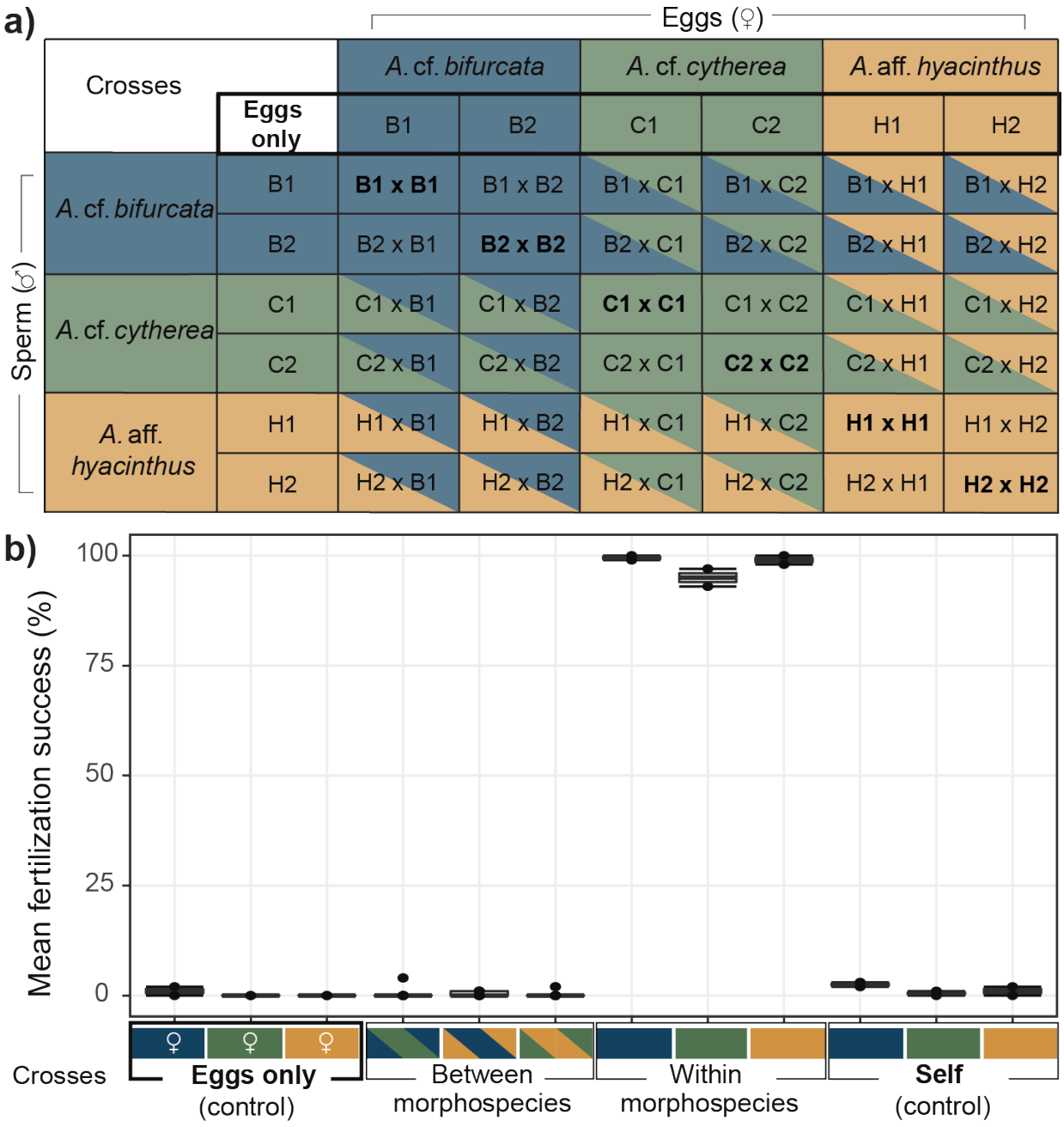

928

929 FIGURE 2.

930

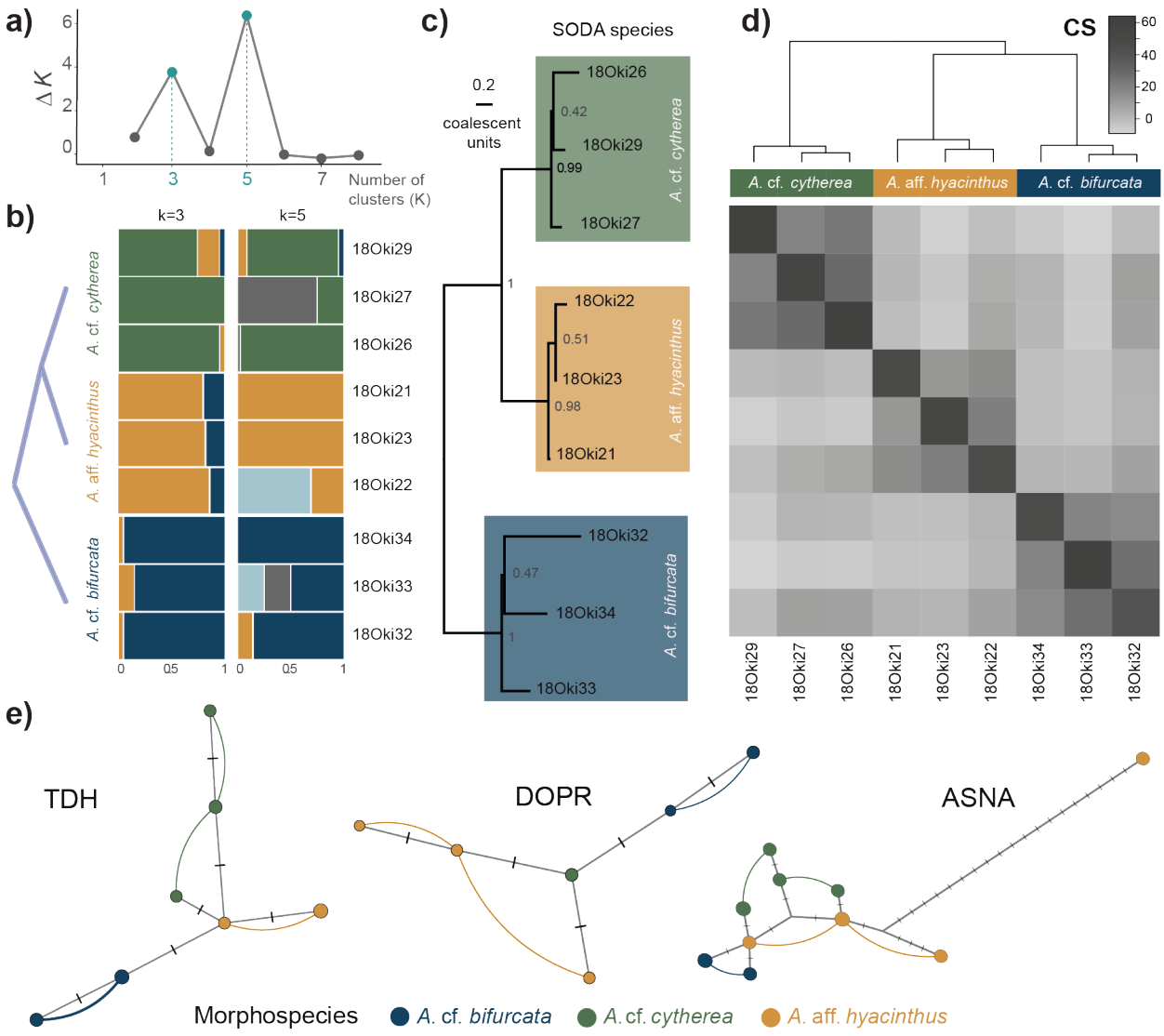

931

932 FIGURE 3.

933

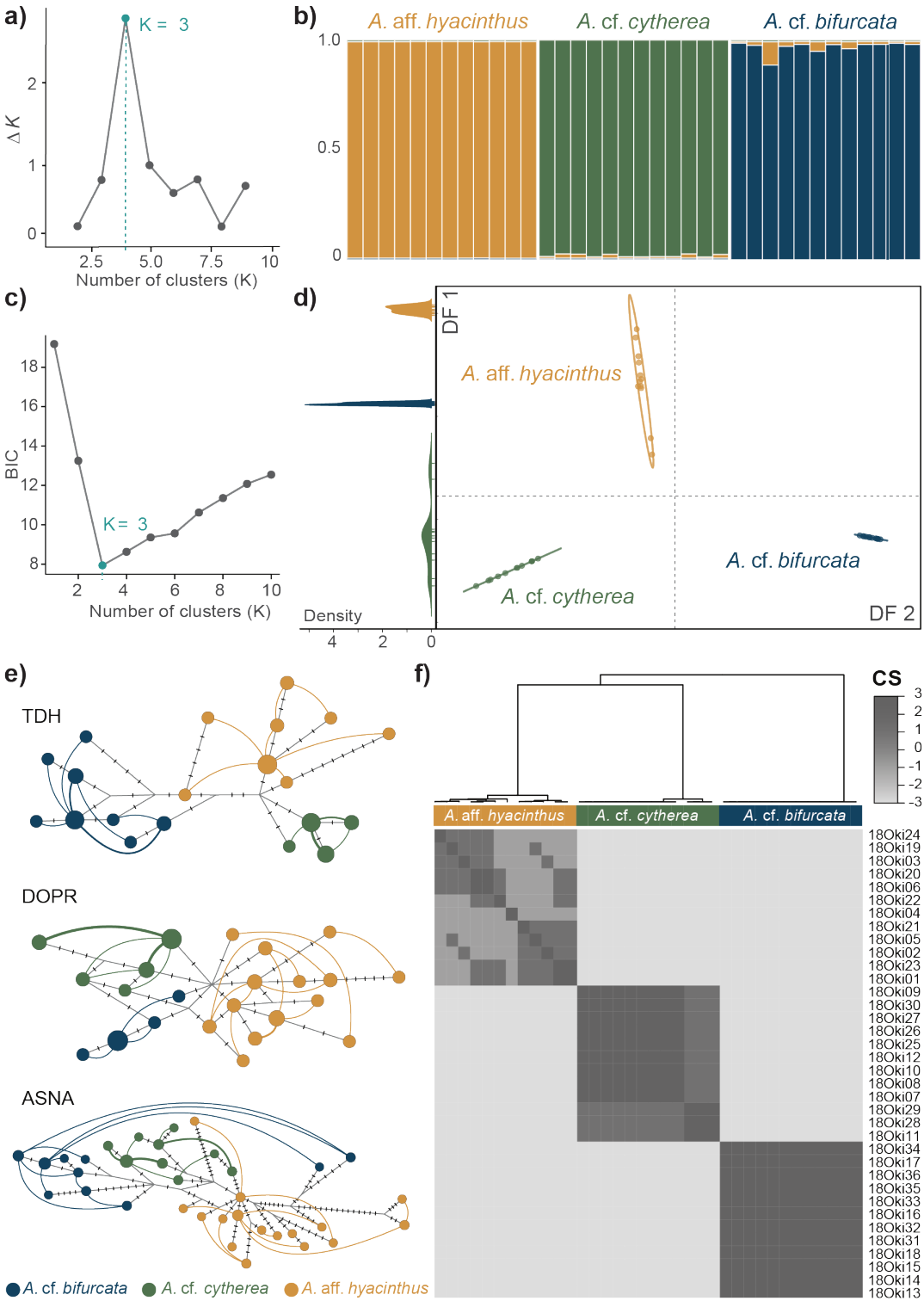

934

935 FIGURE 4.

TABLE 1. A summary of the research into the taxonomic identity of the species used in the study.

Nominal species, authority, accepted name (if different), type locality	**Type material (ID) and current location**	**Type material vs. specimens in this study (ON qual)**	**Ongoing and future perspectives**
Madrepora hyacinthus (Dana 1846), *Acropora hyacinthus*, Fiji	Lectotype (USNM 246) designated by Wallace (1999), deposited at the NMNH, SI (Washington D.C., US)	Distinctive morphological differences between specimens and type material, particularly in branch shape and width ("aff.", affinity with a known species)	Ongoing molecular and morphological comparison to topotypes and other material from the Indo-Pacific
Madrepora cytherea (Dana 1846), *Acropora cytherea,* Tahiti	Lectotype (USNM 423) designated by Wallace (1999), deposited at the NMNH, SI (Washington D.C., US)	Similar morphology, including that of the radial corallites ("cf.", specimens closely resemble type material, but this needs to be confirmed)	Ongoing morphological comparison to lectotypes and molecular comparison to other material from the Indo-Pacific
Acropora bifurcata Nemenzo 1971, Philippines	Holotype (UP C-1295), collected by Nemenzo (1971), deposited at UP, ZD (Quezon City, PH)	Geographical proximity to type location and similar morphology, including radial corallite shape ("cf.", specimens closely resemble type material, but this will require confirmation)	Ongoing molecular and morphological comparison to topotypes and other material from the Indo-Pacific

Catalog numbers from type material (ID) are depicted. Open nomenclature qualifiers (ON qual) were attributed according to the uncertainty degree in identification following Sigovini et al. (2016) and Cowman et al. (2020): *affinis* (aff.) and *confer* (cf.). Refer to "Field Identification and Taxonomic Identity of the Morphospecies" in Materials and Methods for further information. Abbreviations: United States National Museum (USNM), National Museum of Natural History (NMNH), Smithsonian Institution (SI), University of the Philippines (UP), Zoology Department (ZD). Country codes: United States (US), Philippines (PH).

946 **SUPPLEMENTARY MATERIALS**

947

948 TABLE S1. Qualitative (QL) and quantitative (QN) characters used for morphological taxonomic
949 assessment.

Type	No.	Code	Character	(Coding) States / description
QL	1	Color	Colony color in the field	(1) yellow-brown; (2) darker-brown; (3) orange-brown
	2	Bthickness	Relative contribution of corallites to B thickness	(1) axial-dominated; (2) 50/50; (3) radial-dominated
	3	Btaper	Branch taper	(1) tapering; (2) terete
	4	Bradcrowding	Radial crowding (density) along the B	(1) radials do not touch; (2) some radials touch; (3) radials touching
	5	ACshape	Axial corallite dominant shape	(1) tubular; (2) conical; (3) barrel
	6	ACprimaryseprelradius	Relation of AC primary septum to R	(1) <1/4; (2) 1/4 to 3/4; (3) >3/4 R
	7	ACprominentdirectives	Number AC prominent directives	(0) 0; (1) 1; (2) 2
	8	RCshapedominant	RC dominant shape	(1) rounded lip; (2) flaring lip; (3) straight lip
	9	RCsizes	RC sizes	(1) one size; (2) two sizes; (3) mixed; (4) increasing down branch
	10	RCprimaryseprelradius	Relation of RC primary septum to R	(1) <1/4; (2) 1/4 to 3/4; (3) >3/4 R
	11	RCprominentdirectives	Number of RC prominent directives	(0) 0; (1) 1; (2) 2
	12	RCanglebranch	Approximate angle of the RC to the B	(1) 0-30º; (2) 30-60º; (3) 60-90º; (4) 90º
	13	CRtype	Coenosteum type on RC	(1) costate; (2) reticulate; (3) spinous
	14	CRspines	Coenosteum spines on RC	(0) none; (1) simple; (2) forked; (3) elaborate

	15	Ctype	Coenosteum type between RC	(1) costate; (2) reticulate; (3) spinous
	16	Cspines	Coenosteum spines between RC	(0) none; (1) simple; (2) forked; (3) elaborate
	17	B_width	Branch width	Diameter at the base of the B
	18	B_height	Branch height	Distance from tip to base of the B
	19	B_distclosestbranch	Distance to the closest branch	Distance from outer wall of AC to AC outer wall in the nearest B
	20	AC_calyxmaxdiam	Maximum diameter of axial calyx	Maximum distance between inner walls of the AC
	21	AC_maxdiam	Maximum diameter of axial corallite	Maximum distance between outer walls of the AC
QN	22	AC_wallthickness	Axial wall thickness	Difference between maximum diameters of the AC and calyx dived by two (21-20)/2
	23	Ncorallitesbranchdiam	Number of corallites per B	RC per branch diameter at point where B stops tapering
	24	RC_calyxdiamwidestarea	Radial calyx diameter in the widest area	Maximum distance between inner walls of the RC
	25	RC_outerdiamewidestarea	RC diameter in the widest area	Maximum distance between outer walls of the RC
	26	RC_wallthicknesswidestarea	RC wall thickness in the widest area	Wall width at the widest area of the RC
	27	RC_wallthicknesstip	RC wall thickness at the outer tip	Wall width at the outer tip of the RC

Color (No. 1) was assessed from photographs taken from each coral colony. Descriptive characters (2 – 16) were recorded from overall observation of skeletal fragments. Morphometric characters (17 – 19) were measured directly from the branches using Vernier callipers. Corallite features (20 – 27) were obtained using a stereo microscope and an ocular graticule (except for 23 that was counted from above). Character code: branch (B), axial corallite (AC), radial corallite (RC), radius (R).

TABLE S2. Transformation of quantitative morphometric variables.

Type	Code	N (*P*)	H (*P*)	Transformation
QN	B_width	0.0952	0.2637	N/A
	B_height	0.1766	0.1111	N/A
	B_distclosestbranch	0.0755	0.9618	N/A
CT	AC_calyxmaxdiam	<0.001	0.5962	Discretization: 3 L, B= [0.60, 0.78, 0.85, 1.04]
	AC_maxdiam	0.0052	0.5484	Discretization: 4 L, B= [1.34, 1.5, 1.68, 1.85, 2.01]
	AC_wallthickness	0.0002	0.2338	Discretization: 3 L, B= [0.15, 0.20, 0.23, 0.28]
	Ncorallitesbranchdiam	0.0011	0.0230	Discretization: 3 L, B= [5, 7, 9, 12]
	RC_calyxdiamwidestarea	<0.001	0.0214	Discretization: 3 L, B= [0.60, 0.70, 0.85, 1.04]
	RC_outerdiamewidestarea	0.0023	0.2130	Discretization: 3 L, B= [1.04, 1.25, 1.50, 1.79]
	RC_wallthicknesswidestarea	<0.001	0.5247	Discretization: 3 L, B= [0.11, 0.14, 0.18, 0.22]
	RC_wallthicknesstip	<0.001	0.0079	Discretization: 3 L, B= [0.22, 0.28, 0.35, 0.45]

A Shapiro-Wilk test for normality (N) and a Levene test for homogeneity of variances (H) was performed for each quantitative variable with a significance level (α) of 0.05. Quantitative variables that exhibited normal distribution and homoscedasticity ($P>\alpha$) were analyzed as continuous numeric variables (QN). The variables that did not conform to these assumptions (even after applying the optimal transformation using the bestNormalize R package v1.5.0) were discretized into categorical variables according to their distribution (arules R package v1.6-5), and analyzed along with the qualitative characters (CT). Number of levels (L) and breaks (B) are shown for each of those variables.

968
969 TABLE S3. Summary of techniques, loci and methods used in the different stages of the molecular
970 analyses performed in this study.

Stage	Molecular technique	No. loci/markers [n= samples]	Pre-processing		Downstream analyses
Preliminary screening of available molecular markers	PCR-based amplification followed by Sanger sequencing	Three genetic markers (AcroCR, PMCA, FZD) [*n*= 36]	Chromatograms edition, sequence alignment and phasing		Genetic clustering, genetic distances and gene trees
Screening of target-enriched loci	Target enrichment and high-throughput sequencing of conserved elements (exons and UCEs) captured using the hexacoral-v2 bait set	2060 loci (1026 exons, 1034 UCEs) [*n*= 9]	Reads demultiplexing and trimming, contigs assembly and probe matching	Phasing Laninsky pipeline Phasing PHYLUCE pipeline	Genetic clustering (1889 loci), SNAPP species tree (210 loci) Allele sharing-based approaches and extended species trees (79 loci)
Implementation of target-enrichment derived markers in molecular species delimitation	PCR-based amplification followed by Sanger sequencing	Three genetic markers (TDH, DOPR, ASNA) [*n*= 36]	Chromatograms edition, sequence alignment and phasing		Genetic clustering, genetic distances, gene trees, species trees, coalescent and allele sharing-based approaches

971 Detailed information about the techniques, the number of loci, the number of individual samples,
972 and the general pre-processing steps and downstream analyses used at each stage of the molecu-
973 lar approaches used in this study.
974

975

976 TABLE S4. Samples included in the target enrichment sequencing.

Sample ID / Target enrichment ID	SRA accession ID	#C	Mean cov	# Loci (total) UCE / exon	Mean length (bp) UCE / exon
18Oki21 / Acropora_CFhyacinthus1C282	SAMN16242367	17611	22.5	1278 675 /603	1019.7 / 1091.3
18Oki22 / Acropora_CFhyacinthus1C283	SAMN16242368	14902	28.8	1322 680 / 642	1085.9 / 1119.5
18Oki23 / Acropora_CFhyacinthus1C284	SAMN16242369	9907	22.8	1419 717 / 702	895.9 / 949.2
18Oki26 / Acropora_CFcytherea5C285	SAMN16242370	6718	11.3	1686 873 / 813	602.4 / 599.8
18Oki27 / Acropora_CFcytherea5C286	SAMN16242371	8530	21.3	1533 792 / 741	812.1 / 838.6
18Oki29 / Acropora_CFcytherea5C287	SAMN16242372	13314	19.6	1442 731 / 711	1001.4 / 1057.3
18Oki32 / Acropora_CFbifurcataC288	SAMN16242373	23124	38.8	1400 698 / 702	1131.2 / 1183.7
18Oki33 / Acropora_CFbifurcataC289	SAMN16242374	11723	16.2	1465 742 / 723	838.0 / 847.4
18Oki34 / Acropora_CFbifurcataC290	SAMN16242375	15105	23.2	1301 676 / 625	1068.9 / 1132.0

977 Summary of pre-processing statistics of the contigs assembled for the subset of tabular *Acropora*
978 samples. For these samples, target enrichment sequencing was performed using a re-designed set
979 of baits for Hexacorallia that included loci flanking both UCEs and exons (Cowman et al. 2020).
980 Using this target capture approach, 2,060 loci (1,026 exons and 1,034 UCEs) were recovered for
981 the nine samples. Sequence Read Archive (SRA) accession numbers for the raw data are also
982 shown and are gathered under the Bioproject PRJNA665126. Number of contigs (#C), Mean
983 coverage (Mean cov).

984

TABLE S5. Primers and conditions for PCR-based amplification and Sanger sequencing.

Loci (GenBank IDs)	PCR primers (5' - 3')	PCR conditions	Sequencing primers (5' - 3')	Product length (bp)
AcroCR (MT945838 - MT945873)	AcroCR-F[a]: GCCCCTCAAGAGGGTTTCTA AcroCR-R[a]: CTAGACAGGGCCAAGGAGAAG	Ta: 55º 55 cycles	Same as for PCR amplification	1265 – 1352
PMCA (MT945609 - MT945656)	PMCA-F[b]: AAGGAATTGGTGGCTTTCCT PMCA-R[b]: CACAGACGACCATCTTTCCA	Ta: 53º 50 cycles	PMCA-Fint[b]: GAATT-GGTGGCTTTCCTGAG PMCA-Rint[b] : CGAC-CATCTTTCCACTACCTTC	545
FZD (MT945657 - MT945718)	5491-F[b]: TATGGCTGCGACAATTTGGT 5491-R[b]: GCTAGCGTTTCGAGTTCCAC	Ta: 55º 50 cycles	5491-Fint[b]: CCTTGAGTT-GGTTCCTTGCT 5491-Rint[b]: TCGAGTTCCAC-CGTTCTTCT	639
	FZD-F[b]: CCTTGAGTTGGTTCCTTGCT FZD-R[b]: CGCCTAGACAGCAGCTAAAA		Same as for PCR amplification[c]	994 – 1006[d]
TDH (MT945719 - MT945777)	TDH-F[b]: TTTTTCTTTCACTTTT-GGCTGT TDH-R[b]: ATCTCTGCTGCAATCCCAAT	Ta: 53º 50 cycles	Same as for PCR amplification[c]	736 – 744
DOPR (MT945778 - MT945837)	DOPR-F[b]: AGGGTCAGGTTTTTGGGAAT DOPR-R[b]: GAGTTTTGACCGTCAGTTGG	Ta: 53º 50 cycles	Same as for PCR amplification[c]	747 – 760
ASNA (MT945874 - MT945940)	ASNA-F[b]: CTGTGTGCTGGCGAAAAA ASNA-R[b]: GAAAGGCCCCTCTATTTTCA	Ta: 53º 50 cycles	Same as for PCR amplification[c]	748 – 763

[a] Primers designed and tested in-house.

[b] Primers from previous studies (Ladner and Palumbi 2012).

[c] Samples that proved difficult to amplify were re-amplified using M13-tailed PCR primers then sequenced using M13 primers M13F (TGTAAAACGACGGCCAGT) and M13R (CAGGAAACAGCTATGAC).

[d] Product length was extended by assembling contigs using sequences obtained with previously reported primers (Ladner and Palumbi 2012), and sequences obtained using primers designed in-house.

General PCR conditions: start 1 sec 95°C; 1 min 95°C; [30 sec 95°C; 30 sec Tº annealing (Ta); 2 min 72°C]x Number of cycles; 10 min 10°C. GenBank accession numbers (GenBank IDs) for the sequences obtained with each marker are also shown. Different internal primers (int) were used for sequencing in some cases.

TABLE S6. megaBLAST matches for the selected target capture loci and allelic exclusivity screening.

ID dataset	Accession numbers	Description	Code	FFRs gaps as 5th char.	FFRs masked gaps
Exon99029792	XM_029335609	*A. millepora* L-threonine 3-dehydrogenase	TDH	4	3
UCE111109	XM_015902484	*A. digitifera* dopamine receptor 2-like	DOPR	6	3
Exon2711	XM_029333081	*A. millepora* ATPase ASNA1 homolog	ASNA	7	4

The closest megaBLAST hit (accession numbers) is displayed for each of the loci derived from target enrichment sequencing along with a short description that was used to recode them accordingly throughout the text. The number of putative species or fields for recombination (FFRs) they delineated when used in the allele sharing-based approach based (both using gaps as a 5th character or masking them using HaplowebMaker; Spöri and Flot 2020) was used as proxy of their variability and resolution at species-level when compared to the primary species hypotheses (PSHs) derived from morphology.

1010

1011 TABLE S7. *Acropora* genome assemblies used for PCR primer design.

Species	**Assembly version**	**Reference (source)**
A. digitifera (Dana, 1846)	Adig_1.1	Shinzato et al. 2011 (https://www.ncbi.nlm.nih.gov/genome/10529)
A. millepora (Ehrenberg, 1834)	amil_sf_1.1	Ying et al. 2019 (https://www.ncbi.nlm.nih.gov/genome/2652)
A. hyacinthus (Dana, 1846)	Acropora_hyacinthus.discovar_002	Liew et al. 2016, ReFuGe 2020 Consortium 2015 (http://ahya.reefgenomics.org/)
A. palmata (Lamarck, 1816)	Apalm_assembly_v1.0	Kitchen et al. 2019 (requested at: http://baumslab.org/research/data/)
A. cervicornis (Lamarck, 1816)	Acerv_assembly_v1.0	

1012 *Acropora* genome assemblies used to map nuclear loci in order to design primers that maximized
1013 target product length for each region.

1014

1015

1016 TABLE S8. Results of the haploweb allele sharing-based approach to delineate species.

Markers	Feature	Total	Morphospecies		
			A. aff. *hyacinthus*	*A.* cf. *bifurcata*	*A.* cf. *cytherea*
TDH	FFRs	3	1	1	1
	Exclusive alleles	20	8	8	4
	Shared alleles	0	0	0	0
DOPR	FFRs	6	4	1	1
	Exclusive alleles	23	14	4	5
	Shared alleles	0	0	0	0
ASNA	FFRs	9	6	1	2
	Exclusive alleles	35	16	10	9
	Shared alleles	0	0	0	0

1017 Haplowebs delineate putative species according to the fields for recombination (FFRs), or com-
1018 mon allele pools that can be identified. The absence of shared alleles between morphospecies
1019 supports the primary species hypotheses (PSHs) based on morphology, using the criterion of al-
1020 lelic exclusivity as indirect evidence for reproductive isolation.

1021

TABLE S9. Testing alternative species models with the SNAPP coalescence-based approach.

Model	Model description	No. of species	MLE	BF	Rank
1	A single species of tabular *Acropora*	1	-1233.87	-366.13	3
2	Current taxonomy: *A. cytherea* and *A. hyacinthus* (lump *A.* aff. *hyacinthus* + *A.* cf. *bifurcata)*	2	-1050.80	---	2
3	Morphology + breeding trials + genetic clustering: *A.* cf. *cytherea, A.* aff. *hyacinthus* + *A.* cf. *bifurcata*	3	-880.96	339.68**	1

The most likely species models were ranked according to the Bayes factor delimitation (BFD) by calculating the average marginal likelihood estimates (MLE) of five SNAPP-BEAST runs to perform pairwise comparisons between the current taxonomy (model 2) and the alternative species models using Bayes factors (Kass and Raftery 1995):

BF= 2 * [MLEx – MLE1] (see Grummer et al. 2014; Herrera and Shank 2016)

A positive BF value indicates support in favor of the alternative model, while a negative value indicates support of the current taxonomy (model 1) over the alternative one. BF values >10 (**) provide decisive support to distinguish between species models.

1032

1033 TABLE S10. Testing scenarios with different parameter prior distributions in Bayesian species

1034 delimitation using BPP.

ID	Scenario	Parameters	rjMCMC algorithm [parameters]	Most likely number of species [PP]	Best tree topology [PP]
1	Large ancestral population size and deep divergence of species	$\theta \sim IG(3, 0.2)$ mean = 0.1 $\tau_0 \sim IG(3, 0.2)$ mean = 0.1	0 [ε=2]	3 [1.0]	(B, (A, C)) [0.712165]
			1 [α= 2, *m*= 1]	3 [1.0]	(B, (A, C)) [0.630295]
2	Small ancestral population size and shallow divergence of species	$\theta \sim IG(3, 0.002)$ mean = 0.001 $\tau_0 \sim IG(3, 0.002)$ mean = 0.001	0 [ε=2]	3 [1.0]	(A, (B, C)) [0.768815]
			1 [α= 2, *m*= 1]	3 [1.0]	(A, (B, C)) [0.830950]
3	Large ancestral population size and shallow divergence of species[a]	$\theta \sim IG(3, 0.2)$ mean = 0.1 $\tau_0 \sim IG(3, 0.002)$ mean = 0.001	0 [ε=2]	3 [1.0]	(B, (A, C)) [0.435920]
			1 [α= 2, *m*= 1]	3 [1.0]	(B, (A, C)) [0.471725]

1035 [a] Conservative combination of priors (large values for θ and small values for τ_0) that should favor
1036 models with a lower number of species (Leaché and Fujita 2010; McFadden et al. 2017).

1037 Scenarios for testing the influence of three diffuse prior combinations (value 3 for the shape pa-
1038 rameter), with inverse gamma distribution [IG(α, ß)] for population size (θ) and divergence time
1039 at the root of the species tree (τ_0) using Bayesian Phylogenetics and Phylogeography (BPP)
1040 (Yang 2015) for species delimitation. Posterior probabilities [PP] for the most likely number of
1041 species and the best tree topologies out of five runs are shown. Species in the topologies corre-
1042 spond to A) *A.* aff. *hyacinthus*, B) *A.* cf. *bifurcata*, C) *A.* cf. *cytherea.*
1043

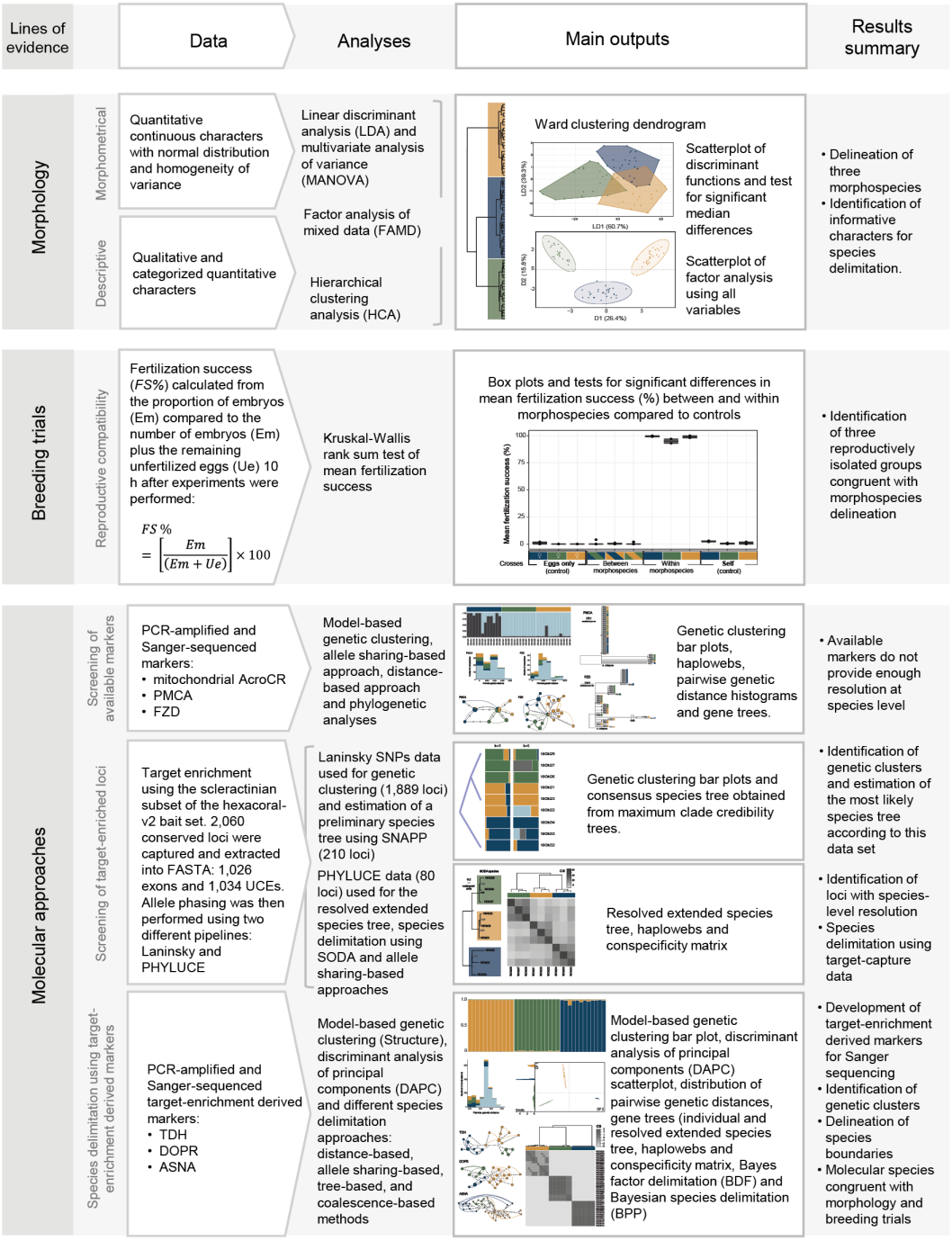

FIGURE S1. Multiple lines of evidence used to delineate species boundaries in the tabular *Acropora* from Sesoko Island (Okinawa, Japan). A summarized workflow of the lines of evidence used in this study is presented. The data used, the analyses, the main outputs and a brief summary of the results are shown.

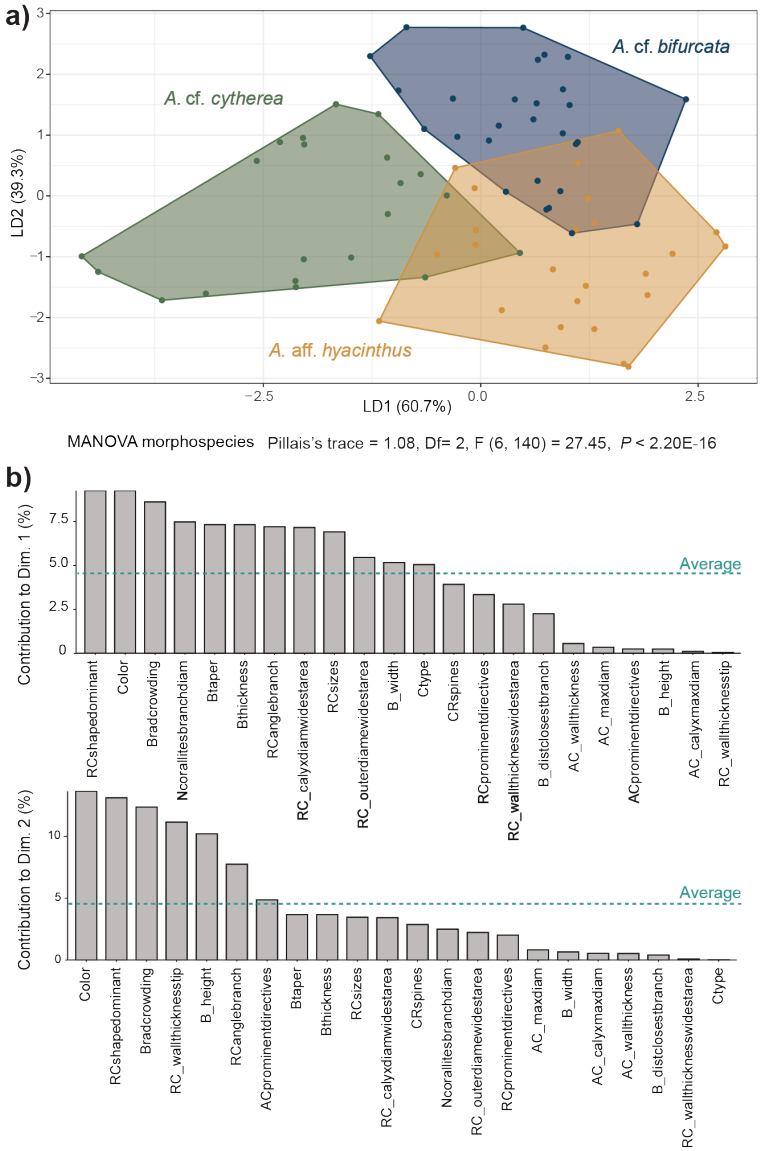

FIGURE S2. Multivariate analyses of morphological characters. a) Linear discriminant analysis (LDA) of continuous variables exhibiting 81.08% accuracy in discriminating between morphospecies (n= 74): B_width (r = 0.49, P < 0.001), B_height (r = 0.51, P<0.001) and B_distclosestbranch (r = 0.19, P < 0.001). The result of a one-way MANOVA test for these variables is also displayed. Additionally, statistically significant differences between species were found when using post-hoc univariate ANOVA tests for each dependent variable (n= 74, P < 0.001 for each, see details in Dataset S1). b) Individual contribution (%) of each character to the mapping dimensions 1 (left) and 2 (right) of the FAMD. Each variable code corresponds to those described in Tables S1 and S2. The dashed lines indicate the average contribution value (%) for each dimension.

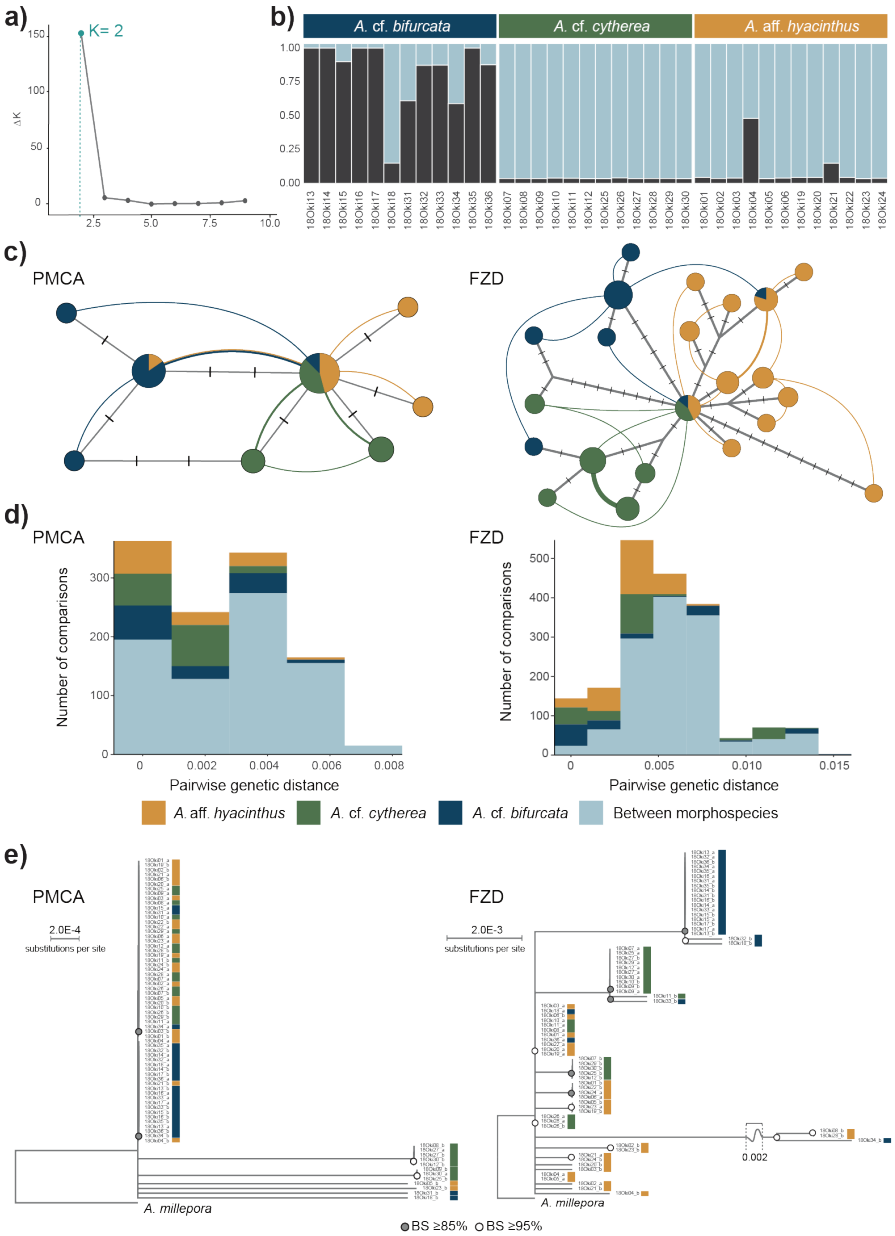

FIGURE S3. Preliminary screening of PMCA and FZD markers. a) Evanno ΔK plot suggesting the most likely K value (dashed line) for model-based genetic clustering. b) STRUCTURE plot obtained by assigning the probability of individual membership with K=2. b) Allele sharing-based haplowebs with shades corresponding to the groups delineated by morphology and breeding trials. c) Histograms of pairwise comparison of genetic distances within and between morphospecies. d) Ultrafast bootstrap trees for each phased marker with bootstrap support (BS) of 85-94% indicated by grey and BS ≥ 95% by white circles at the corresponding nodes. Alleles for each individual are differentiated by the suffixes "_a" and "_b".

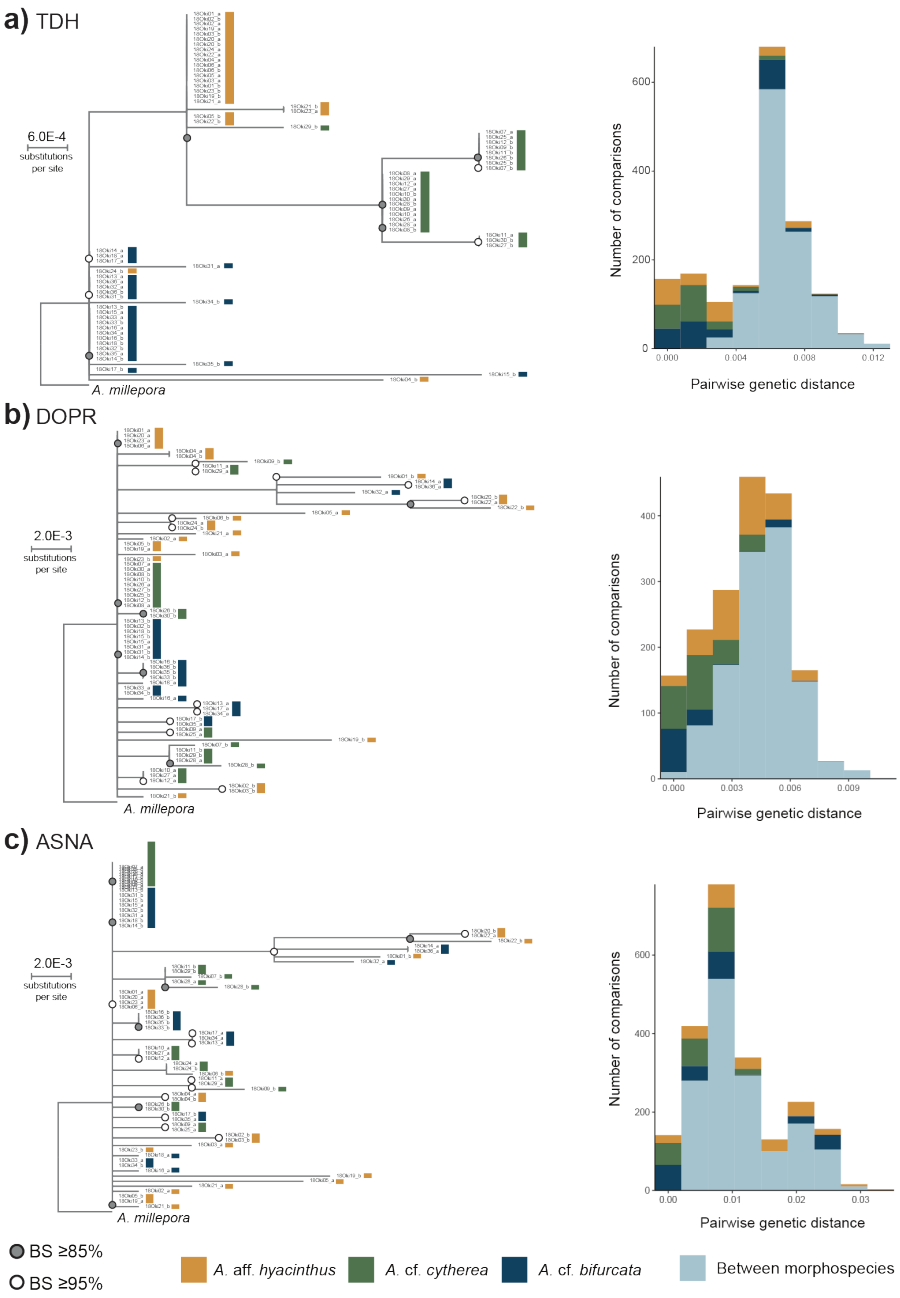

FIGURE S4. Phylogenetic trees and genetic distance histograms for each marker derived from target-capture sequencing. Ultrafast bootstrap trees and pairwise genetic distances comparison within and between morphospecies for markers defined from target-capture sequencing: a) TDH, b) DOPR and c) ASNA. In the trees, nodes with less than 85% of support were collapsed whereas bootstrap support (BS) of 85 to 94% is indicated by grey and 95% by white circles at the corresponding nodes. Alleles of each individual are differentiated by the suffixes "_a" and "_b".

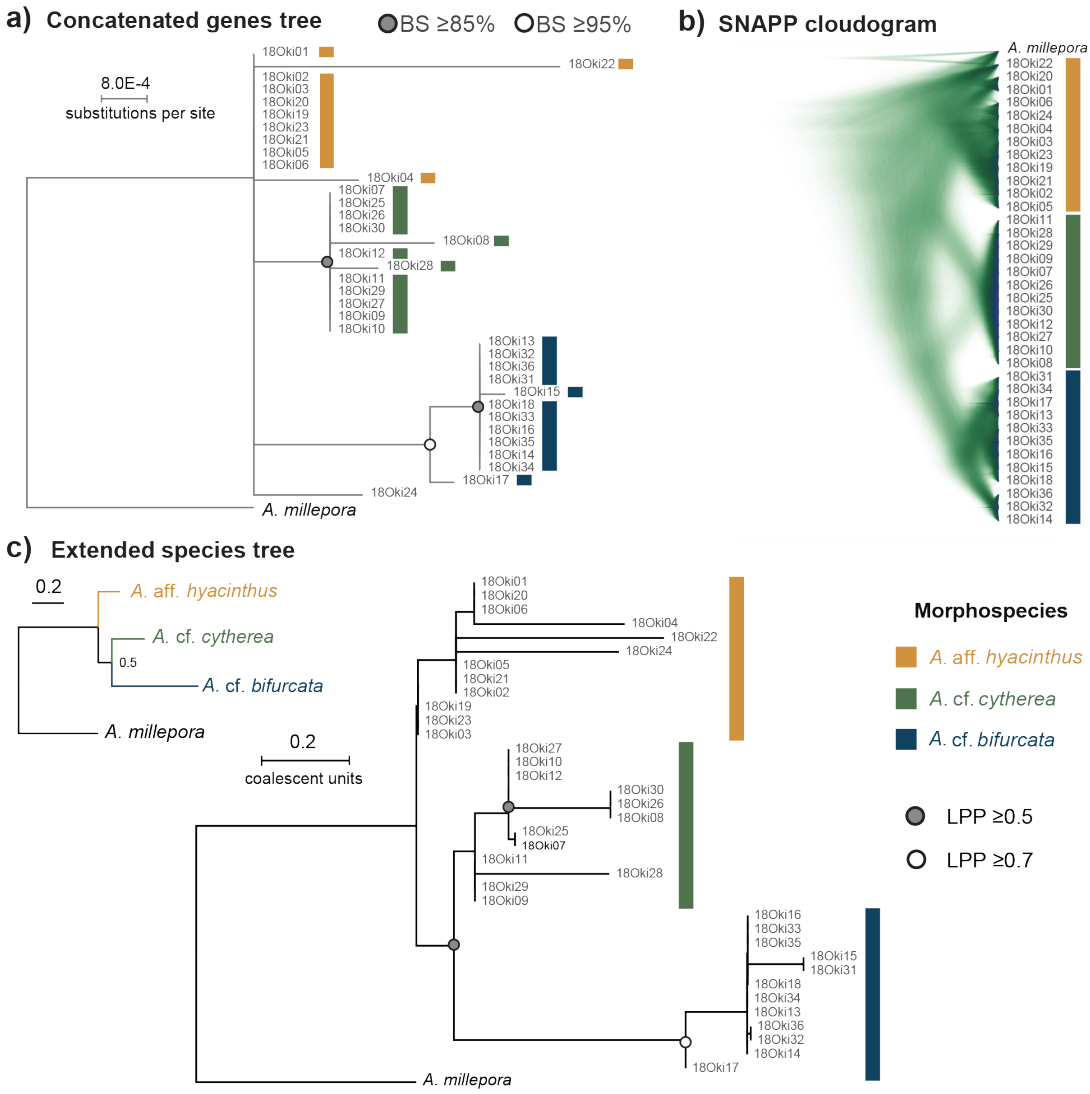

FIGURE S5. Concatenated gene and species trees for the three target enrichment-derived markers. Phylogenetic trees of three target capture derived loci (TDH, DOPR and ASNA) shaded according to the primary species hypotheses (PSHs) regarding to morphospecies. a) Ultrafast bootstrap tree for the concatenated IUPAC consensus sequences of the three markers. Nodes with less than 85% of bootstrap support (BS) were collapsed. b) SNAPP cloudogram using SNP information extracted from the target enrichment defined markers, where each individual was allowed to be a terminal tip (i.e. without constraining individuals into species). c) ASTRAL extended species trees obtained by mapping alleles to individuals, where both morphospecies were monophyletically constrained (inset) and left unconstrained (main tree, resolved extended species trees). Nodes with less than 10% of local posterior probability (LPP) were collapsed.

REFERENCES

Cowman P.F., Quattrini A.M., Bridge T.C., Watkins-Colwell G.J., Fadli N., Grinblat M., Roberts T.E., McFadden C.S., Miller D.J., Baird A.H. 2020. An enhanced target-enrichment bait set for Hexacorallia provides phylogenomic resolution of the staghorn corals (Acroporidae) and close relatives. Mol. Phylogenetics Evol. 153:106944.

Grummer J.A., Bryson R.W., Reeder T.W. 2014. Species delimitation using Bayes factors: Simulations and application to the *Sceloporus scalaris* species group (Squamata: Phrynosomatidae). Syst. Biol. 63:119–133.

Herrera S., Shank T.M. 2016. RAD sequencing enables unprecedented phylogenetic resolution and objective species delimitation in recalcitrant divergent taxa. Mol. Phylogenetics Evol. 100:70–79.

Kass R.E., Raftery A.E. 1995. Bayes factors. J. Am. Stat. Assoc. 90:773–795.

Kitchen S.A., Ratan A., Bedoya-Reina O.C., Burhans R., Fogarty N.D., Miller W., Baums I.B. 2019. Genomic variants among threatened *Acropora* corals. G3 Genes, Genomes, Genet. 9:1633–1646.

Ladner J.T., Palumbi S.R. 2012. Extensive sympatry, cryptic diversity and introgression throughout the geographic distribution of two coral species complexes. Mol. Ecol. 21:2224–2238.

Leaché A.D., Fujita M.K. 2010. Bayesian species delimitation in West African forest geckos (*Hemidactylus fasciatus*). Proc. R. Soc. B Biol. Sci. 277:3071–3077.

Liew Y.J., Aranda M., Voolstra C.R. 2016. Reefgenomics.Org – a repository for marine

genomics data. Database.

McFadden C.S., Haverkort-Yeh R., Reynolds A.M., Halàsz A., Quattrini A.M., Forsman Z.H., Benayahu Y., Toonen R.J. 2017. Species boundaries in the absence of morphological, ecological or geographical differentiation in the Red Sea octocoral genus *Ovabunda* (Alcyonacea: Xeniidae). Mol. Phylogenet. Evol. 112:174–184.

ReFuGe 2020 Consortium. 2015. The ReFuGe 2020 Consortium – using "omics" approaches to explore the adaptability and resilience of coral holobionts to environmental change. Front. Mar. Sci. 2:68.

Shinzato C., Shoguchi E., Kawashima T., Hamada M., Hisata K., Tanaka M., Fujie M., Fujiwara M., Koyanagi R., Ikuta T., Fujiyama A., Miller D.J., Satoh N. 2011. Using the *Acropora digitifera* genome to understand coral responses to environmental change. Nature. 476:320–323.

Spöri Y., Flot J.-F. 2020. HaplowebMaker and CoMa: two web tools to delimit species using haplowebs and conspecificity matrices. Methods Ecol. Evol. 11:1434–1438.

Yang Z. 2015. The BPP program for species tree estimation and species delimitation. Curr. Zool. 61:854–865.

Ying H., Hayward D.C., Cooke I., Wang W., Moya A., Siemering K.R., Sprungala S., Ball E.E., Forêt S., Miller D.J. 2019. The whole-genome sequence of the coral *Acropora millepora*. Genome Biol. Evol. 11:1374–1379.